(12) INTERNATIONAL APPLICATION PUBLISHED UNDER THE PATENT COOPERATION TREATY (PCT)

(19) World Intellectual Property Organization
International Bureau

(43) International Publication Date
06 September 2024 (06.09.2024)

WIPO | PCT

(10) International Publication Number
WO 2024/182216 A2

(51) International Patent Classification:
Not classified

(21) International Application Number:
PCT/US2024/016980

(22) International Filing Date:
23 February 2024 (23.02.2024)

(25) Filing Language: English

(26) Publication Language: English

(30) Priority Data:
63/448,654 27 February 2023 (27.02.2023) US

(71) Applicant: **MERCK SHARP & DOHME LLC** [US/US]; 126 East Lincoln Avenue, Rahway, New Jersey 07065 (US).

(72) Inventors: **KASPER, Stephen H.**; 126 East Lincoln Avenue, Rahway, New Jersey 07065 (US). **CASSADAY, Jason A.**; 126 East Lincoln Avenue, Rahway, New Jersey 07065 (US). **OTTEN, Stephanie**; 126 East Lincoln Avenue, Rahway, New Jersey 07065 (US). **SQUADRONI, Brian**; 126 East Lincoln Avenue, Rahway, New Jersey 07065 (US).

(74) Agent: **SUH, Su Kyung**; 126 East Lincoln Avenue, Rahway, New Jersey 07065 (US).

(81) Designated States *(unless otherwise indicated, for every kind of national protection available)*: AE, AG, AL, AM, AO, AT, AU, AZ, BA, BB, BG, BH, BN, BR, BW, BY, BZ, CA, CH, CL, CN, CO, CR, CU, CV, CZ, DE, DJ, DK, DM, DO, DZ, EC, EE, EG, ES, FI, GB, GD, GE, GH, GM, GT, HN, HR, HU, ID, IL, IN, IQ, IR, IS, IT, JM, JO, JP, KE, KG, KH, KN, KP, KR, KW, KZ, LA, LC, LK, LR, LS, LU, LY, MA, MD, MG, MK, MN, MU, MW, MX, MY, MZ, NA, NG, NI, NO, NZ, OM, PA, PE, PG, PH, PL, PT, QA, RO, RS, RU, RW, SA, SC, SD, SE, SG, SK, SL, ST, SV, SY, TH, TJ, TM, TN, TR, TT, TZ, UA, UG, US, UZ, VC, VN, WS, ZA, ZM, ZW.

(84) Designated States *(unless otherwise indicated, for every kind of regional protection available)*: ARIPO (BW, CV, GH, GM, KE, LR, LS, MW, MZ, NA, RW, SC, SD, SL, ST, SZ, TZ, UG, ZM, ZW), Eurasian (AM, AZ, BY, KG, KZ, RU, TJ, TM), European (AL, AT, BE, BG, CH, CY, CZ, DE, DK, EE, ES, FI, FR, GB, GR, HR, HU, IE, IS, IT, LT, LU, LV, MC, ME, MK, MT, NL, NO, PL, PT, RO, RS, SE, SI, SK, SM, TR), OAPI (BF, BJ, CF, CG, CI, CM, GA, GN, GQ, GW, KM, ML, MR, NE, SN, TD, TG).

Declarations under Rule 4.17:

— *as to the identity of the inventor (Rule 4.17(i))*
— *as to applicant's entitlement to apply for and be granted a patent (Rule 4.17(ii))*
— *as to the applicant's entitlement to claim the priority of the earlier application (Rule 4.17(iii))*

(54) **Title:** INTRACELLULAR DELIVERY OF COMPOUNDS IN MULTIPLEXED CELL-BASED ASSAYS

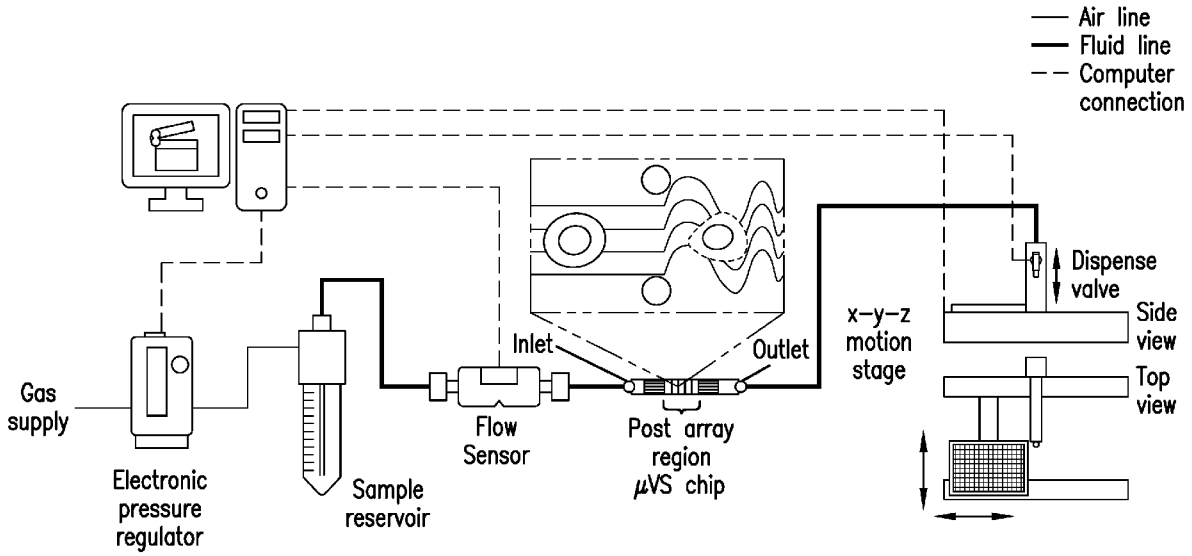

FIG.2A

(57) **Abstract:** Systems and methods are provided for introducing exogenous material into cells in a fast, multiplexed manner in vitro using mechanoporation, *e.g.*, microfluidic vortex shedding or cell squeezing.

WO 2024/182216 A2

[Continued on next page]

Published:

— *without international search report and to be republished upon receipt of that report (Rule 48.2(g))*

— *with sequence listing part of description (Rule 5.2(a))*

INTRACELLULAR DELIVERY OF COMPOUNDS IN MULTIPLEXED CELL-BASED ASSAYS

FIELD

[0001] This disclosure relates generally to the field of microfluidic technologies and high-throughput cell assays for intracellular delivery of molecules.

CROSS-REFERENCE TO RELATED APPLICATIONS

[0002] This application claims the benefit of U.S. Provisional Patent Application No. 63/448,654, filed February 27, 2023, which is incorporated by reference herein its entirety.

REFERENCE TO SEQUENCE LISTING SUBMITTED ELECTRONICALLY

[0003] The instant application contains a Sequence Listing which has been submitted electronically in XML format and is hereby incorporated by reference in its entirety. The XML file, created on May 4, 2023, is named 25661-WO-PCT-SEQLIST.XML and is 59.6 KB in size.

BACKGROUND OF THE INVENTION

[0004] Enabling intracellular delivery (ICD) of impermeable molecules has the potential to facilitate and accelerate multiple aspects of biological research, yet it presents with important challenges. ICD has historically been achieved through many approaches, including electroporation, vector-mediated transfer, and mechanoporation, the process of transferring molecules into cells using mechanical energy (Stewart et al., 2016, 2018). Recent advances in microfluidic methods have enabled novel mechanoporation, including nanoneedle penetration, micro/nanoinjection, cell squeezing, cell stretching, and fluid shearing (Hur and Chung, 2021). These methods have shown the ability to efficiently deliver various cargos into a wide range of cells, often with minimal cell perturbation. However, the low throughput of these techniques, primarily due to the requirement for pre-mixing cells with the cargo of interest prior to microfluidic processing, has been a significant bottleneck toward leveraging these techniques in cell-based screens supporting drug discovery efforts.

[0005] Cyclic peptides are a compelling modality to target notoriously difficult-to-drug intracellular protein-protein interactions (PPIs), due to their size and ability to bind flat PPI interfaces with exceptional affinity and selectivity ((Morioka et al., 2015; Buyanova and Pei, 2022). Combinatorial cyclic peptide libraries are particularly well-suited for discovering potent binders of difficult intracellular PPIs (Philippe et al., 2021). However, conducting structure

activity relationship (SAR) studies with these molecules is fraught with challenges as these molecules typically do not have sufficient cell permeability and do not follow normal drug-likeness conventions (*e.g.*, Lipinski's rule of five (Lipinski et al., 2001)). This lack of cell permeability is due to their size and hydrophilicity (Bashiruddin and Suga, 2015; Qian et al., 2017; Dougherty et al., 2019). Therefore, there is often a disconnect in potency between biochemical assays and cell-based assays, making the discovery of cyclic peptides for intracellular PPIs a major challenge (Hochman et al., 2021). Indeed, out of 18 cyclic peptides approved for clinical use in the past two decades – only two, romidepsin and voclosporin, modulate intracellular targets (Zhang and Chen, 2022).

[0006] There is a currently a significant effort toward improving the drug-like properties of macrocyclic peptides, including cellular permeability (Walport et al., 2017; Vinogradov et al., 2019). In addition to modifying the peptides themselves, advances in targeted delivery via nanocarriers (El-Sayed et al., 2005; Solaro et al., 2010; Tong et al., 2020; Manzari et al., 2021; Doty et al., 2022), cell-penetrating peptides (Dougherty et al., 2019), antibody-drug conjugates (Moldenhauer et al., 2012), and more, may enable formulation-based strategies to deliver peptides intracellularly to engage with targets of interest that may be difficult to drug with small molecules.

[0007] Microfluidic-based mechanoporation and subsequent ICD can be a useful approach to study intracellular target engagement of cyclic peptides without the use of exogenous transfection reagents or electrical fields. Microfluidic vortex shedding (μVS) is a fluid shearing-based technique that was recently demonstrated to be effective at delivering mRNA and Cas9 ribonucleoprotein into primary human T cells (Jarrell et al., 2019, 2021). μVS is induced when fluid flows past micron-scale posts (40 μm diameter with 20 μm gaps) to create turbulent oscillating flow motion, which disrupts the lipid membrane (Renfer et al., 2013; Jarrell et al., 2019). Advantages of μVS over other microfluidic intracellular delivery approaches are the high flow rate and reduced clogging events, which are a function of the geometry that accompany the desired cell-permeabilizing hydrodynamic conditions. However, the ability to use μVS to screen large numbers of large molecules in a highly multiplexed manner is untenable, as molecules to be screened must be pre-mixed with cells for testing. Testing or screening molecules using multiple types of molecules, the same molecule in multiple concentrations, or multiple combinations of molecules requires mixing up desired test condition and applying to individual batches of cells, which can be time-consuming.

[0008] Microfluidic cell squeezing has previously been reported for target engagement studies with poorly permeable small molecules (Janus kinase inhibitors), although those studies suffered from low throughput and analytical capability (Li et al., 2017).

[0009] There is a need for a vector-free intracellular delivery approach with suitable throughput for cell-based assay screening in order to build knowledge around functional target engagement of impermeable molecules, *e.g.*, cyclic peptides, in a native cellular environment.

SUMMARY OF THE INVENTION

[0010] The present disclosure provides systems and methods for multiplex in vitro delivery of exogenous material in cells.

[0011] In a first aspect, the disclosure provides a system for multiplexed in vitro delivery of exogenous material into at least one cell suspended in a liquid, the system comprising: a) a microfluidic device having a flow channel configured to disrupt a membrane of the at least one cell and allow the exogenous material to enter the disrupted cell membrane; b) a sample reservoir in liquid communication with the microfluidic device, the sample reservoir containing a mixture of at least one cell and liquid; c) a flow sensor positioned between the sample reservoir and the microfluidic device, the flow sensor in liquid communication with the sample reservoir and the microfluidic device; d) an electronic pressure regulator in gaseous communication with the sample reservoir and a gas supply, wherein the electronic pressure regulator is configured to move the liquid and at least one cell through the flow sensor, into the microfluidic device, and along the flow channel; e) a dispensing valve in fluid communication with the microfluidic device and in fluid communication with a dispensing tip; f) an X-Y-Z motorized stage positioned underneath the dispensing tip, the X-Y-Z motorized stage configured to hold a microplate having wells containing liquid and exogenous material; and g) one or more processors and a memory coupled with the one or more processors, the memory storing instructions which, when executed by the processor, can open and close the dispensing valve and move the X-Y-Z motorized stage, wherein the one or more processors are in data communication with the flow sensor, the electronic pressure regulator, the dispensing valve, and the X-Y-Z motorized stage.

[0012] In some embodiments of the first aspect, the flow channel of the microfluidic device includes at least two flow diverters, and the gap between the at least two flow diverters has a width greater than the diameter of the cell. In some embodiments of the first aspect, the flow channel of the microfluidic device includes at least one cell-deforming constriction wherein the diameter of the constriction is from about 20 to about 60% of the diameter of the cell.

[0013] In a second aspect, the disclosure provides a method for multiplexed in vitro delivery of exogenous material into at least one cell suspended in a liquid comprising: a) adding gaseous pressure to a sample reservoir containing the liquid and the at least one cell; b) moving a dispensing tip above a first microplate well, wherein the dispensing tip is in liquid communication with a dispensing valve and the dispensing valve is in liquid communication with the sample reservoir; c) opening the dispensing valve to move the liquid and the at least one cell through a flow sensor due to the gaseous pressure; d) detecting the flow rate of the liquid, sending detected flow rate data to a processor, and calculating a cumulative flow of the liquid; and e) closing the dispensing valve when the cumulative flow of the liquid through the flow sensor has reached a volume such that the at least one cell has flowed through a microfluidic device having a flow channel configured to disrupt a membrane of the at least one cell, through the dispensing valve and the dispensing tip, and into the first microplate well containing the exogenous material.

[0014] In some embodiments of the second aspect, the flow channel of the microfluidic device includes at least two flow diverters, and the gap between the at least two flow diverters has a width greater than the diameter of the cell. In some embodiments of the second aspect, the flow channel of the microfluidic device includes at least one cell-deforming constriction wherein the diameter of the constriction is from about 20 to about 60% of the diameter of the cell.

[0015] In some embodiments of the second aspect, the method comprises a step of moving the dispensing tip to a second microplate well.

[0016] In some embodiments of the first or second aspects, the exogenous material is one or more cell-impermeable molecules. In some embodiments of the first or second aspects, the exogenous material is selected from the group consisting of: a composition having one or more active pharmaceutical ingredients; a molecular glue; a deubiquitinase-targeting chimera; a lysosome-targeting chimaera for degradation of extracellular proteins; an autophagy-targeting chimera; an autophagosome-tethering compound; a phosphorylation-targeting chimera; and a ribonuclease targeting chimera degrader.

[0017] In some embodiments of the first or second aspects, the exogenous material is selected from the group consisting of: an inorganic compound; a drug; a nucleic acid; a plasmid; a protein; a carbohydrate; and a synthetic polymer. In some embodiments of the first or second aspects, the exogenous material is a proteolysis-targeting chimera molecule. In some embodiments of the first or second aspects, the exogenous material is a cyclic peptide.

[0018] The summary of the technology described above is non-limiting and other features and advantages of the technology will be apparent from the following detailed description, and from the claims.

BRIEF DESCRIPTION OF THE FIGURES

[0019] FIGS. 1A-1F show the induction of a short window of cell permeability after μVS-processing. FIG. 1A is a schematic diagram of processing for cells that are pre-mixed with fluorescently-labeled dextran (average molecular weight = 3 kDa). FIG. 1B is a schematic representation of processing for cells that are mixed with labeled dextran post-μVS-processing ("post-mixed"). FIG. 1C is a bar graph showing the delivery efficiency of AF-488-dextran into HeLa cells in pre- and post-mixed formats using μVS as determined by flow cytometry. FIG. 1D is a scatter plot of membrane resealing kinetics of HeLa cells after μVS-processing. FIG. 1E is a bar graph showing the delivery efficiency of AF-488-dextran into HCT116 cells in pre- and post-mixed formats using μVS. FIG. 1F is a scatter plot of membrane resealing kinetics of HCT116 cells after μVS-processing.

[0020] FIGS. 2A-2I shows an overview of a dispensing microfluidic vortex shedding (DμVS) system and characterization of dispensing. FIG. 2A is a component diagram of the DμVS system. An electronic pressure regulator controls the applied pressure to a cell suspension in the sample reservoir. When activated, cell suspension flows through the flow sensor, then the μVS chip where permeability is induced, then the dispense valve, and finally to the designated well on a microplate. System components are controlled by a proprietary in-house automation software package, Telios. FIG. 2B is a flowchart of the software logic feedback loop. FIG. 2C is a line graph of flow rate during dispensing into a 96-well plate. An entire 96-well plate can be filled in under 2.5 min when 100 μl is dispensed into each well. FIG. 2D is a line graph of flow rate (20 ms resolved) during DμVS filling into an individual well of a 96-well plate. Flow rate is rapidly increased when valve opens and stopped when valve is closed. Valve is open for ~700 ms for 100 μl fill. FIG. 2E is a line graph of flow rate (20 ms resolved) during DμVS filling into an individual well of a 384-well plate. Valve is open for ~300 ms for 40 μl fill. FIG. 2F is a dot plot of plate-wide fluorescence for FD20 solution (cell-free) dispensed from DμVS into a 96-well plate. FIG. 2G is a dot plot of plate-wide fluorescence for CELLTRACKER™-labeled HeLa cells DμVS-processed into a 96-well plate. FIG. 2H is a dot plot of plate-wide fluorescence for FD20 solution (cell-free) dispensed from DμVS into a 384-well plate. FIG. 2I is a dot plot of plate-wide fluorescence for CELLTRACKER™ labeled HeLa cells DμVS-processed into a 384-

well plate. In FIGS. 2F-2I, plate-wide average is indicated by the black horizontal line and dotted lines represent SD. The %CV values are indicated on each individual graph.

[0021] FIGS. 3A-3H show DμVS-enhanced ICD of cyclic peptides characterized with NANOCLICK™ assay. FIG. 3A is a schematic diagram of how the NANOCLICK™ assay is used to quantify relative peptide delivery enhancement of DμVS. In FIG. 3A, NANOLUC®-HALOTAG® expressing Hela cells are treated with dibenzoazacyclooctyne-chloroalkane (DIBAC-CA) (i), after which these cells are transferred to 96-well plates containing cyclic azido-peptides either by standard pipetting or DμVS dispensing (ii). After incubation, cells are treated with NB618-Az (iii) and then BRET signal is measured upon addition of NANOLUC® substrate (iv). Increased azido-peptide delivery leads to a decreased BRET signal. FIG. 3B is a scatterplot for a dose response curve of Peptide 1 and Peptide 2 in the NANOCLICK™ assay without cell permeabilization (unprocessed). FIG. 3C is a scatterplot for a dose response curve of Peptide 1 and Peptide 2 in the NANOCLICK™ assay with DμVS processing. FIG. 3D is a scatterplot for a dose response curve of Peptide 1 and Peptide 2 in the NANOCLICK™ assay with digitonin treatment (lytic). FIG. 3E is a schematic diagram of the plate map design for the data shown in FIGS. 3F-3H, with each well represented by a larger circle. Wells with a white diamond inside them represent vehicle, wells with a white circle inside them represent 30 μM Peptide 1, and wells with a white square inside them represent 30 μM Peptide 2. FIG. 3F is a dot plot of aggregate NANOBRET® data for cells without permeabilization (unprocessed, FIG. 3F) and with DμVS processing (FIG. 3G). Diamonds represent vehicle, circle represent 30 μM Peptide 1, and white square represent 30 μM Peptide 2. The CV values for DμVS processed cells were: 3.52% for vehicle treatment, 3.24% for Peptide 1 and 5.01% for Peptide 2. FIG. 3H is a dot plot of data from FIG. 3G plotted by well position on the plate. Data were fitted with a linear regression model and 95% confidence interval is shown (solid and dotted lines, respectively). Diamonds represent vehicle, circle represent 30 μM Peptide 1, and white square represent 30 μM Peptide 2.

[0022] FIGS. 4A-4F show data demonstrating that DμVS enables an impermeable cyclic peptide to drive a functional response in a p53 reporter assay. FIG. 4A is a dot plot of the 96-well format p53 reporter assay in unprocessed and DμVS conditions. The ratiometric readout normalizes p53-controlled β-lactamase activity (460 nm) to total cell number (530 nm). Z-prime values for both assay formats are shown beneath the x-axis. FIG. 4B is a scatter plot of the dose response curves of Peptide 1 and Peptide 2 in the unprocessed 96-well assay format. FIG. 4C is a scatter plot of the dose response curves of Peptide 1 and Peptide 2 in the DμVS 96-well assay format. FIG. 4D is a dot plot of the 384-well format p53 reporter assay in unprocessed and DμVS conditions. Z-prime values for both assay formats are shown beneath the x-axis. FIG. 4E is a

scatter plot of the dose response curves of Peptide 1 and Peptide 2 in the unprocessed 384-well assay format. FIG. 4F is a scatter plot of the dose response curves of Peptide 1 and Peptide 2 in the DμVS 384-well assay format.

[0023] FIGS. 5A-5D show DμVS-p53 reporter screening data for additional p53/MDM2 cyclic peptides. FIG. 5A is a bar graph of activity of 17 peptides at 10 μM in the p53 reporter assay with and without DμVS. Cyclic peptides were reordered on graph into three classes: (i) activity unchanged between methods, (ii) DμVS-improved activity, and (iii) no activity in either method. (b, c, d) Selected dose response curves of validated hits in the DμVS-p53 reporter assay: Peptide 7 (b), Peptide 6 (c), and Peptide 8 (d). The EC_{50} value displayed on the graph is from the DμVS-based assay format.

[0024] FIG. 6 shows the flow rates at various pressures.

[0025] FIG. 7 depicts normalized cytotoxicity for each applied pressure.

DETAILED DESCRIPTION OF THE DISCLOSURE

[0026] To improve on the existing throughput of μVS methodologies, the inventors integrated a μVS chip with inline microplate-based dispensing (dispensing microfluidic vortex shedding; DμVS). The inventors designed and constructed the DμVS system to rapidly shuttle permeabilized cells to standard microplates containing various payloads at different concentrations. The inventors then validated the DμVS method using p53/MDM2 peptides in both a click-chemistry-based permeability assay (NANOCLICK™, 96-well format), as well as a functional p53 reporter assay (96- and 384-well format).

Definitions

[0027] Listed below are definitions of various terms used herein. These definitions apply to the terms as they are used throughout this specification and claims, unless otherwise limited in specific instances, either individually or as part of a larger group.

[0028] Unless defined otherwise, all technical and scientific terms used herein have the same meaning as commonly understood by one of ordinary skill in the art. Generally, the nomenclature used herein and the laboratory procedures in cell culture, molecular genetics, organic chemistry, and peptide chemistry are those well-known and commonly employed in the art.

[0029] As used herein, the articles "a" and "an" refer to one or to more than one (i.e., to at least one) of the grammatical object of the article. By way of example, "an element" means one element or more than one element. Furthermore, use of the term "including" as well as other forms, such as "include," "includes," and "included," is not limiting.

[0030] As used herein, the term "about" in quantitative terms refers to plus or minus up to 10% of the value it modifies (rounded up to the nearest whole number if the value is not sub-dividable, such as a number of molecules or nucleotides).

[0031] All ranges disclosed herein are inclusive of the recited endpoints and independently combinable (for example, the range of "from 50 mg to 500 mg" is inclusive of the endpoints, 50 mg and 500 mg, and all the intermediate values and ranges therein).

[0032] As used herein, the term "comprising" may include the embodiments "consisting of" and "consisting essentially of." The terms "comprise(s)," "include(s)," "having," "has," "may," "contain(s)," and variants thereof, as used herein, are intended to be open-ended transitional phrases, terms, or words that require the presence of the named ingredients/steps and permit the presence of other ingredients/steps. However, such description should be construed as also describing compositions or processes as "consisting of" and "consisting essentially of" the enumerated components, which allows the presence of only the named components or compounds, along with any acceptable carriers or fluids, and excludes other components or compounds.

[0033] As used herein, the term "microfluidic device" refers to a device that has one or more micrometer- or nanometer-scale channels to allow for the manipulation and control of fluids confined in the channels.

[0034] As used herein, the term "flow channel" refers to a micrometer- or nanometer-scale channel within a microfluidic device.

[0035] As used herein, the term "flow sensor" refers to an electronic device that measures the rate of flow of a liquid.

[0036] As used herein, the term "electronic pressure regulator" refers to an electronic device that can control the flow of a pressurized gas.

[0037] As used herein, the term "dispensing valve" refers to a valve that can be opened and closed to dispense liquid through a dispensing tip into a microplate well.

[0038] As used herein, the term "X-Y-Z motorized stage" refers to a motorized stage that can hold a multi-well microplate and move the microplate along the X, Y, and Z axes to position individual wells of the microplate underneath a dispensing tip and allow dispensing of liquid from the dispensing tip.

[0039] As used herein, the term "mechanoporation" refers to techniques of cell membrane disruption via physical means and subsequent intracellular delivery of exogenous materials within microfluidic confinement. Mechanical forces, through fluid shear, physical contact, microneedles, or acoustics, disrupt the lipid bilayer membrane of cells, creating nanopores or

nanoholes in the cellular membrane (Hur and Chung, 2021). Nearby external molecules then diffuse into the cell through the membrane nanopores.

Abbreviations

[0040]	DMSO	dimethyl sulfoxide
[0041]	FAM	fluorescein amidite
[0042]	FBS	fetal bovine serum
[0043]	FEP	fluorinated ethylene-propylene
[0044]	ID	inner diameter
[0045]	ms	millisecond(s)
[0046]	OD	outer diameter
[0047]	PBS	phosphate buffered saline
[0048]	psi	pounds per square inch
[0049]	PTFE	PolyTetraFluoroEthylene
[0050]	SBS	Society for Biomolecular Screening

Mechanoporation

[0051] Mechanoporation of cells for intracellular delivery of molecules can be accomplished using a variety of methods, including fluid shearing deformation, constriction (squeezing; see, *e.g.*, US10696944B2), poking, microinjection or nanoinjection, sonoporation, laser cavitation, and electroporation, some of which can be combined (*e.g.*, constriction and electroporation) (Hur and Chung, 2021). Within each of these general techniques, there can be multiple methods of generating the mechanical forces needed to disrupt the cell membrane. For example, mechanoporation via fluid shearing deformation may be accomplished using flow diverters within a flow channel to generate liquid vortices (*e.g.*, vortex shedding; see US Patent No. 11268060B2) or cross-junction microfluidic channels that can generate vortices (Hur and Chung, 2021).

[0052] Microfluidic vortex shedding chips were used in the examples of this disclosure to mechanoporate cells. However, without being bound by theory, the inventors hypothesize that other mechanoporation techniques described above (such as constriction) may be used with the system components of this disclosure to attain a multiplexing of multiple conditions for impermeable molecules.

Exogenous materials

[0053] Many cell-impermeable molecules may be used with the multiplexed DμVS methods described herein. Exemplary cell-impermeable molecules include, but are not limited to: an inorganic compound; a drug; a nucleic acid; a plasmid; a protein; a carbohydrate; a synthetic polymer; a pharmaceutical composition including compositions having one or more active pharmaceutical ingredients; a molecular glue such as proteolysis-targeting chimera molecules (PROTACs; Békés et al., 2022); deubiquitinase-targeting chimeras (DUBTACs; Henning et al., 2022); lysosome-targeting chimaeras for degradation of extracellular proteins (LYTACs); autophagy-targeting chimeras (AUTACs); autophagosome-tethering compounds (ATTECs); phosphorylation-targeting chimeras (PhosTACs); and ribonuclease targeting chimera degraders (RIBOTACs).

[0054] In some embodiments, the exogenous material is one or more cell-impermeable molecules. In some embodiments, the exogenous material is selected from the group consisting of: a composition having one or more active pharmaceutical ingredients; a molecular glue; a deubiquitinase-targeting chimera; a lysosome-targeting chimaera for degradation of extracellular proteins; an autophagy-targeting chimera; an autophagosome-tethering compound; a phosphorylation-targeting chimera; and a ribonuclease targeting chimera degrader. In some embodiments, the exogenous material comprises a composition having one or more active pharmaceutical ingredients. In some embodiments, the exogenous material comprises a molecular glue. In some embodiments, the exogenous material comprises a deubiquitinase-targeting chimera. In some embodiments, the exogenous material comprises a lysosome-targeting chimaera for degradation of extracellular proteins. In some embodiments, the exogenous material comprises an autophagy-targeting chimera. In some embodiments, the exogenous material comprises an autophagosome-tethering compound. In some embodiments, the exogenous material comprises a phosphorylation-targeting chimera. In some embodiments, the exogenous material comprises a ribonuclease targeting chimera degrader.

[0055] In some embodiments, the exogenous material is selected from the group consisting of: an inorganic compound; a drug; a nucleic acid; a plasmid; a protein; a carbohydrate; and a synthetic polymer. In some embodiments, the exogenous material comprises an inorganic compound. In some embodiments, the exogenous material comprises a drug. In some embodiments, the exogenous material comprises a nucleic acid. In some embodiments, the exogenous material comprises a plasmid. In some embodiments, the exogenous material comprises a protein. In some embodiments, the exogenous material comprises a carbohydrate. In some embodiments, the exogenous material comprises a synthetic polymer.

[0056] In some embodiments, the exogenous material comprises a proteolysis-targeting chimera molecule. In some embodiments, the exogenous material comprises a cyclic peptide.

Systems or methods for delivery of exogenous material into a cell

[0057] In some embodiments, the system comprises a microfluidic device having a flow channel configured to disrupt a membrane of the at least one cell and allow the exogenous material to enter the disrupted cell membrane. In some embodiments, the system comprise a sample reservoir in liquid communication with the microfluidic device, the sample reservoir containing a mixture of at least one cell and liquid. In some embodiments, a flow sensor positioned between the sample reservoir and the microfluidic device, the flow sensor in liquid communication with the sample reservoir and the microfluidic device. In some embodiments, the system comprises an electronic pressure regulator in gaseous communication with the sample reservoir and a gas supply. In some embodiments, the electronic pressure regulator is configured to move the liquid and at least one cell through the flow sensor, into the microfluidic device, and along the flow channel. In some embodiments, the system comprise a dispensing valve in fluid, communication with the microfluidic device and in fluid communication with a dispensing tip. In some embodiments, the system comprises an X-Y-Z motorized stage positioned underneath the dispensing tip, the X-Y-Z motorized stage configured to hold a microplate having wells containing liquid and exogenous material. In some embodiments, the system comprises one or more processors and a memory coupled with the one or more processors, the memory storing instructions which, when executed by the processor, can open and close the dispensing valve and move the X-Y-Z motorized stage, wherein the one or more processors are in data communication with the flow sensor, the electronic pressure regulator, the dispensing valve, and the X-Y-Z motorized stage.

[0058] In some embodiments, the method for multiplexed in vitro delivery of exogenous material into at least one cell suspended in a liquid comprises adding gaseous pressure to a sample reservoir containing the liquid and the at least one cell. In some embodiments, the method comprises moving a dispensing tip above a first microplate well. In some embodiments, the dispensing tip is in liquid communication with a dispensing valve and the dispensing valve is in liquid communication with the sample reservoir. In some embodiments, the method comprises opening the dispensing valve to move the liquid and the at least one cell through a flow sensor due to the gaseous pressure. In some embodiments, the method comprises detecting the flow rate of the liquid, sending detected flow rate data to a processor, and calculating a cumulative flow of the liquid. In some embodiments, the method comprises closing the dispensing valve when the

cumulative flow of the liquid through the flow sensor has reached a volume such that the at least one cell has flowed through a microfluidic device having a flow channel configured to disrupt a membrane of the at least one cell, through the dispensing valve and the dispensing tip, and into the first microplate well containing the exogenous material.

[0059] In some embodiments, the method comprises moving the dispensing tip to a second microplate well.

[0060] In some embodiments, the flow channel of the microfluidic device includes at least two flow diverters. In some embodiments, the gap between the at least two flow diverters has a width greater than the diameter of the cell.

[0061] In some embodiments, the flow channel of the microfluidic device includes at least one cell-deforming constriction. In some embodiments, the diameter of the constriction is from about 20 to about 60% of the diameter of the cell. In some embodiments, the diameter of the constriction is from about 20 to about 50% of the diameter of the cell. In some embodiments, the diameter of the constriction is from about 20 to about 40% of the diameter of the cell. In some embodiments, the diameter of the constriction is from about 20 to about 30% of the diameter of the cell. In some embodiments, the diameter of the constriction is from about 30 to about 60% of the diameter of the cell. In some embodiments, the diameter of the constriction is from about 40 to about 60% of the diameter of the cell. In some embodiments, the diameter of the constriction is from about 50 to about 60% of the diameter of the cell. In some embodiments, the diameter of the constriction is from about 30 to about 40% of the diameter of the cell. In some embodiments, the diameter of the constriction is from about 40 to about 50% of the diameter of the cell. In some embodiments, the diameter of the constriction is about 20% of the diameter of the cell. In some embodiments, the diameter of the constriction is about 30% of the diameter of the cell. In some embodiments, the diameter of the constriction is about 40% of the diameter of the cell. In some embodiments, the diameter of the constriction is about 50% of the diameter of the cell. In some embodiments, the diameter of the constriction is about 60% of the diameter of the cell.

[0062] In some embodiments, the system is operated at a pressure within the range of 0.5 PSI to 200 PSI. In some embodiments, the system is operated at a pressure within the range of 0.75 PSI to 200 PSI. In some embodiments, the system is operated at a pressure within the range of 1 PSI to 200 PSI. In some embodiments, the system is operated at a pressure within the range of 0.5 PSI to 150 PSI. In some embodiments, the system is operated at a pressure within the range of 0.5 PSI to 120 PSI. In some embodiments, the system is operated at a pressure within the range of 0.5 PSI to 100 PSI. In some embodiments, the system is operated at a pressure within the range of 0.5 PSI to 90 PSI. In some embodiments, the system is operated at a pressure within the

range of 0.5 PSI to 80 PSI. In some embodiments, the system is operated at a pressure within the range of 0.5 PSI to 70 PSI. In some embodiments, the system is operated at a pressure within the range of 0.5 PSI to 60 PSI. In some embodiments, the system is operated at a pressure of at least 0.4 PSI. In some embodiments, the system is operated at a pressure of at least 0.5 PSI. In some embodiments, the system is operated at a pressure of at least 0.6 PSI. In some embodiments, the system is operated at a pressure of at least 0.7 PSI. In some embodiments, the system is operated at a pressure of at least 0.75 PSI.

[0063] In some embodiments, the gaseous pressure is within the range of 0.5 PSI to 200 PSI. In some embodiments, the gaseous pressure is within the range of 0.75 PSI to 200 PSI. In some embodiments, the gaseous pressure is within the range of 1 PSI to 200 PSI. In some embodiments, the gaseous pressure is within the range of 0.5 PSI to 150 PSI. In some embodiments, the gaseous pressure is within the range of 0.5 PSI to 120 PSI. In some embodiments, the gaseous pressure is within the range of 0.5 PSI to 100 PSI. In some embodiments, the gaseous pressure is within the range of 0.5 PSI to 90 PSI. In some embodiments, the gaseous pressure is within the range of 0.5 PSI to 80 PSI. In some embodiments, the gaseous pressure is within the range of 0.5 PSI to 70 PSI. In some embodiments, the gaseous pressure is within the range of 0.5 PSI to 60 PSI. In some embodiments, the gaseous pressure is at least 0.4 PSI. In some embodiments, the gaseous pressure is at least 0.5 PSI. In some embodiments, the gaseous pressure is at least 0.6 PSI. In some embodiments, the gaseous pressure is at least 0.7 PSI. In some embodiments, the gaseous pressure is at least 0.75 PSI.

EXAMPLES

[0064] The following examples are meant to be illustrative and should not be construed as further limiting. The contents of the figures and all references, patents, and published patent applications cited throughout this application are expressly incorporated herein by reference.

Example 1: μVS enhances delivery of 3 kDa dextran and induces a short window of cell permeability after processing.

[0065] To explore the possibility of using μVS for the intracellular delivery of cyclic peptides (~700-2000 Daltons), the inventors used μVS to deliver ALEXAFLUOR™-488-labeled 3 kDa dextran (AF-488-dextran) into HeLa and HCT116 cells. Cells were pre-mixed with AF-488-dextran and processed through μVS at 120 psi (FIG. 1A), then monitored delivery by flow cytometry. Unsurprisingly, as μVS has previously been shown to deliver much larger

macromolecular cargoes (Jarrell et al., 2019, 2021), there was a substantial increase in the number of dextran-positive cells (94.5 ± 5.2% and 85.0 ± 15.1%, in HeLa and HCT116, respectively) after μVS processing as compared to unprocessed cells treated with AF-488-dextran alone (3.3 ± 0.2% and 3.5 ± 1.5%, in HeLa and HCT116, respectively) (FIGS. 1C and 1E).

[0066] The inventors sought to determine if cells maintain permeability after exiting the μVS chip. Therefore the inventors tested μVS-induced intracellular delivery by mixing with AF-488-dextran with cells immediately post-processing (FIG. 1B). Since the flow rate through the device was ~8 ml/min and the dead volume of the exit tubing was ~100 μl, the cells were expected to come into contact with the payload in ~0.75 secs. Surprisingly, there was only a very slight loss of delivery efficiency in both cell types using this approach (85.9 ± 7.5% and 81.5 ± 9.0%, in HeLa and HCT116, respectively) compared with the pre-mixing methodology (FIGS. 1C and 1E). This is a similar timescale of membrane resealing observed after cell squeezing (Sharei et al., 2014)).

[0067] Importantly, there was minimal loss of cell viability in μVS-processed cells (ranging from ~15-23% viability loss in HeLa, and ~1.7-8.5% in HCT116; data not shown). This minimal loss of cell viability is at a level similar to previous reports with μVS (Jarrell et al., 2019, 2021), as well as another microfluidic cell shearing method (Kizer et al., 2019), and cell constriction (Sharei et al., 2013, 2015; Han et al., 2015; DiTommaso et al., 2018).

[0068] The inventors next sought to determine the rate at which cells reseal following collection. For these experiments, cells were processed similarly to the post-mix conditions described above and AF-488-dextran was then added at various timepoints post-collection. Both HeLa and HCT116 cells rapidly resealed with a dramatic loss in delivery efficiency after several minutes (FIGS. 1D and 1F). When fitted to a one-phase decay model, HeLa displayed a resealing $t_{1/2}$ of 2.8 min ($R^2 = 0.9029$) and HCT116 resealed with $t_{1/2}$ of 1.1 min ($R^2 = 0.9020$). Taken together, these data suggest that μVS can permeabilize cells to efficiently deliver low molecular weight macromolecules, and that cell membrane impermeability is re-established within minutes.

Example 2: Design of the DμVS system to integrate microfluidic cell mechanoporation with multiplexed cell-based assays.

[0069] The experiments of Example 1 defined a brief time window allowing delivery of permeabilized cells to respective payloads but cautions of an exponential tradeoff of delivery efficiency with time. Because μVS is performed at a high flow rate (~8 ml/min) and the dead volume of tubing downstream of the chip is relatively low (~100-200 μl), the inventors realized

that permeabilized cells can be delivered a multiplex of payloads with minimal loss in delivery efficiency if the right fluidic handling is built around it.

[0070] Given the potential utility of μVS to drug discovery, the inventors sought to build a system capable of vector-free ICD that is scaled to be compatible with microplate-based screening methods. Since the delivery efficiency of μVS-processed cells rapidly decreases after collection, the inventors devised a strategy to quickly deliver permeabilized cells to multiple cargoes as quickly as feasible. Therefore, the inventors converted the manual and labor-intensive process of microfluidic sample handling to create a multiplexed (semi-)automated process, by means of combining plate-based dispensing with μVS (DμVS) (FIG. 2A). Four computer-controlled components were added to the microfluidic method: (1) an electronic pressure regulator upstream of the sample reservoir, (2) a flow sensor downstream of the sample reservoir and just upstream of the μVS chip, (3) a microsolenoid valve-based dispense tip on a z-motor downstream of the chip, and (4) an x-y motor stage that can accommodate and maneuver a standard microplate beneath the dispense tip (FIG. 2A). All four components were synchronized and controlled through proprietary automation software called Telios (Cassaday et al., 2017). The electronic pressure regulator allows the user to choose and initiate the applied pressure at the start of an experimental run. The inline flow sensor provides rapid flow feedback to the system, thereby controlling for two phenomena that can occur when cell suspensions pass through microfluidic chips at this size scale and flow regime: (1) very fast clogging/unclogging events at high frequency and (2) slow clogging from accumulation of cells/debris within the chip. The dispense valve allows for precise stopping of the flow and the x-y stage can then move the microplate into position beneath the dispense tip.

[0071] The basic logic process operated by the Telios system is shown in the flowchart in FIG. 2B. The user uploads an operations file, which indicates the target volume for each well, and indicates the desired pressure for cell processing. Once the user initiates DμVS, the rest of the process is automated via Telios. The dispense valve is put into the closed state and the desired pressure is applied. The x-y stage positions the microplate so that the first well is beneath the dispense tip and the valve is opened. As the cell suspension flows through the system, the flow rate data is fed back to the software via the flow sensor in 20 ms loops. After the target volume is achieved, the dispense valve is closed, the x-y stage positions the next well under the dispense tip, and the valve is opened to repeat the process. The flow rate data is logged throughout the process (FIGS. 2C-2E).

[0072] To characterize the accuracy of this semi-automated process, the inventors processed a cell-free solution of 20 kDa FITC-dextran (FD20) into both 96- and 384-well plates and then

measured the percent coefficients of variation (%CV) in fluorescent signal (FIGS. 2F and 2H; 96-well = 6.1% CV, 384-well = 3.5% CV). The fluid was processed with an applied pressure of 120 psi to mimic the conditions where cell permeability is achieved (as illustrated herein and in previous reports; Jarrell et al., 2019, 2021). Likewise, the inventors characterized the well-to-well consistency of processing and dispensing a cell suspension at 120 psi.

[0073] In this case, fluorescently labeled HeLa cells were DμVS-processed to 96- and 384-well plates, and the resulting fluorescence was recorded across the plate (FIGS. 2G and 2I; 96-well = 8.5% CV, 384-well = 4.7% CV). These results indicate that the DμVS configuration, with the added components to semi-automate and increase the multiplexing ability and throughput of μVS, can achieve good well-to-well dispensing homogeneity of solutions and cell suspensions that undergo hydrodynamic conditions that are conducive to mechanoporation.

Example 3: Intracellular delivery of cyclic peptides into DμVS-processed cells.

[0074] To characterize DμVS-based intracellular delivery of peptides in a high-throughput amenable cell-based permeability assay, the inventors employed the NANOCLICK™ assay (Peier et al., 2021). NANOCLICK™ is a target-agnostic permeability assay that utilizes in-cell copper-free click chemistry (Jewett and Bertozzi, 2010), HALOTAG® labeling (Los et al., 2008), and NANOBRET® technology (Machleidt et al., 2015) (FIG. 3A). The inventors selected for analysis two azido-analogs of ATSP-7041 (Chang et al., 2013), a peptide that targets the PPI between two cytoplasmic proteins, p53 and MDM2: (1) Peptide 1, a cell-permeable positive control peptide with MDM2 binding K_D of 19 nM (biochemical) and EC_{50} of 0.42 μM in the p53 reporter assay (cellular) (Partridge et al., 2019), and (2) Peptide 2, a cell-impermeable peptide that shows high-affinity binding to MDM2 (K_D = 2.3 nM) but does not display cellular activity in the p53 reporter assay (EC_{50} > 50 μM; FIG. 3B; Peier et al., 2021).

[0075] HeLa cells expressing a NANOLUC®-HALOTAG® construct were treated with DIBAC-CA so that the HALOTAG® domain reacts with the chloroalkane linker, rendering close proximity of the DIBAC group and NANOLUC® domain (FIG. 3A, [i]). These cells were then processed by DμVS directly into plates containing pre-plated peptides (FIG. 3A, [ii]). In parallel, unprocessed cells (non-permeabilized control) and cells treated with digitonin (lytic control) were exposed to the same peptide conditions as the DμVS-processed cells. When azido-peptides enter the cell, they undergo a strain-promoted azide-alkyne click reaction with the DIBAC group on the NANOLUC®-HALOTAG® construct. Cells were then treated with the azido-modified NANOBRET® fluorophore (NB618-Az), which reacts with any remaining unoccupied DIBAC groups (FIG. 3A, [iii]). Thus, a BRET signal is generated in inverse proportion to the amount of

cytosolic peptide (FIG. 3A, [iv]). When cells were unprocessed, Peptide 1 showed moderate permeability while Peptide 2 showed no permeability, similarly to previous observations (Peier et al., 2021) (FIGS. 3C and 3D).

[0076] However, when cells were processed through the DμVS system, a dose-dependent reduction in BRET signal was observed with both azido-peptides, demonstrating intracellular delivery and 'click' reactivity with the DIBAC groups (Peptide 1 EC_{50} = 0.24 μM, Peptide 2 EC_{50} = 1.14 μM; FIGS. 3C and 3D). As a positive control, the inventors used a lytic format of the assay where cells were treated with digitonin, a detergent that permeabilizes the cell membrane. With this treatment, the inventors also observed dose-dependent BRET signal inhibition for both peptides (Peptide 1 EC_{50} = 0.09 μM, Peptide 2 eC_{50} = 0.99 μM; FIGS. 3C and 3D).

[0077] While the EC_{50} values for both peptides were similar between DμVS and the lytic assay formats, the lytic treatment contributed a greater max inhibition of BRET signal (~73% lytic versus ~40% DμVS). This was likely the result of the timescale of permeability, where DμVS induces transient porosity that rapidly reseals within several minutes whereas digitonin induces sustained permeability throughout the entire assay incubation.

[0078] After observing the DμVS-induced enhanced delivery of azido-peptides in a dose-dependent fashion, the inventors utilized the NANOCLICK™ assay to characterize azido-peptide delivery efficiency as a function of position on the plate. The inventors sought to understand any variance that the DμVS process might introduce in this cell-based assay and determine if there are any locational effects. The inventors plated high concentrations of both Peptide 1, Peptide 2, as well as DMSO (vehicle) as shown in FIG. 3E. The permeabilized cells were dispensed to the full 96-well plate within 130 seconds (data not shown). In the unprocessed control the inventors observed %CV of 3.53% for vehicle treatment, 3.43% for Peptide 1 and 2.79% for Peptide 2 (FIG. 3F). For DμVS, the observed %CVs were 3.52% for vehicle treatment, 3.24% for Peptide 1 and 5.01% for Peptide 2 (FIG. 3G). This suggests that DμVS processing has very little effect on the intrinsic variability of the assay (unchanged variation in the vehicle and Peptide 1 treatments). In addition, the location on the plate had little impact on the variance of cytosolic delivery of Peptide 2 via DμVS (well number vs NANOBRET® R^2 = 0.1549; FIG. 3H).

[0079] These data suggest that DμVS can be used for robust, repeatable intracellular delivery of cyclic peptides.

Example 4: Peptide 2 exhibits cellular activity after DμVS processing in p53 reporter assay.

[0080] Next, the inventors sought to determine if DμVS delivery is sufficient to drive a functional effect toward disrupting the p53/MDM2 PPI. For these experiments, the inventors leveraged an HCT116-based cell line containing a β-lactamase reporter gene that is responsive to p53 activity. This assay has previously been used to characterize the cellular activity of p53/MDM2 peptides, including Peptide 1 and Peptide 2, where Peptide 1 displayed good cell potency (EC_{50} = 0.42 μM) and Peptide 2 showed no activity (Partridge et al., 2019; Peier et al., 2021). The assay, which is typically performed on adherent cells, was adapted to accommodate the DμVS process where cells must be in suspension to flow through the device.

[0081] Similar to the NANOCLICK™ assay above, cells were DμVS-processed directly onto pre-plated peptides. After incubation, cells were treated with a Fluorescence Resonance Energy Transfer (FRET)-based fluorescent β-lactamase substrate to generate a ratiometric readout of p53-regulated gene expression per cell number. In 96-well format, the assay performed well with the above modifications, as both the unprocessed cells (cells in suspension but not flowed through DμVS) and the DμVS-processed cells displayed good Z-prime scores when comparing vehicle treatment (negative control) with a high concentration of Peptide 1 (positive control; FIG. 4A). In the unprocessed conditions (i.e., no DμVS) Peptide 1 and Peptide 2 had similar potencies as described in previous reports (Partridge et al., 2019; Peier et al., 2021) (FIG. 4B; Peptide 1 EC_{50} = 0.36 μM, Peptide 2 EC_{50} > 30 μM).

[0082] Following DμVS processing however, Peptide 2 showed a clear dose response and low-micromolar potency (EC_{50} = 2.4 μM; FIG. 4C), while the potency of the permeable Peptide 1 was largely unchanged (EC_{50} = 0.49 μM). These data indicate that this high-affinity MDM2-binder is capable of properly engaging the target and driving efficacy in the native cell environment when its cellular permeability is increased. The intracellular delivery of Peptide 2 was especially encouraging, as it is highly-negatively charged (-6 net charge), due to having three glutamic acid residues flanked at both the C- and N-termini.

[0083] After showing that the DμVS system yields robust, correlative results in two cell-based assays in 96-well format, the inventors wanted to test whether the throughput of DμVS could be further increased by performing the p53-reporter assay in a 384-well format. In this higher throughput format, six replicates of dose titrations for each peptide could be tested.

[0084] Similar to the 96-well format, the assay showed good signal-to-noise and Z-prime values with the necessary accommodations to implement DμVS (FIG. 4D). The unprocessed conditions also yielded expected results (FIG. 4E; Peptide 1 EC_{50} = 0.47 μM, Peptide 2 EC_{50} >

30 μM). However, similar to the inventor's observations in the 96-well format, Peptide 2 showed a large increase in activity in a dose-dependent manner when cells undergo DμVS processing (EC_{50} = 0.95 μM; FIG. 4F), whereas Peptide 1 activity was unaffected (EC_{50} = 0.35 μM; FIG. 4F).

Example 5: Variable activity of p53/MDM2 cyclic and linear peptides in a cellular context.

[0085] The inventors next sought to determine the generalizability of the DμVS technique across different p53/MDM2 peptides that have a broad range of activities in both the non-permeabilized p53 reporter assay and a cell-free MDM2-binding.the inventors assessed an additional 15 peptides from previously reported literature (Hu et al., 2007; Liu et al., 2010; Phan et al., 2010; Brown et al., 2013; Chang et al., 2013; Partridge et al., 2019), including a non-binding cyclic peptide as a negative control (Peptide 17). Table 1 below lists the sequences of the cyclic peptides used.

Table 1: Sequences

SEQ ID NO.	Peptide Name	Sequence
1	Peptide 1	Ac-Lys(N_3)-betaAla-Leu-Thr-Phe-R8*-Glu-Tyr-Trp-Ala-Gln-Cba-S5*-Ser-Ala-Ala-NH_2
2	Peptide 3	Ac-Lys(N_3)-betaAla-Leu-Thr-Phe-R8*-Glu-Tyr-Trp-Ala-Gln-Cba-S5*-Glu-Ala-Ala-Ala-Ala-DAla-NH_2
3	Peptide 4	Ac-Lys(N_3)-betaAla-Leu-Thr-Phe-R8*-Glu-Tyr-Trp-Ala-Gln-Cba-S5*-Ala-DAla-Ala-DAla-Ala-DAla-NH_2
4	Peptide 5	H-R5*-DAla-DTrp(6-F)-DTyr-B5**-DAsn-DPhe(4-CF3)-DGlu-DLys-DLeu-DLeu-R8*-DAla-DAla-DAla-DAla-DAla-DAla-NH_2
5	Peptide 2	NH2-Glu-Glu-Glu-Lys(N_3)-Ser-Gly-Ser-Thr-Ser-Phe-E8*-Glu-Tyr-Trp-Ala-Leu-Leu-S5*-Glu-Glu-Glu-NH_2
6	Peptide 7	NH2-Glu-Glu-Glu-Lys(N_3)-Ser-Gly-Ser-Thr-Ser-Phe-R8*-Glu-Tyr-Trp-Ala-Leu-Leu-S5*-NH_2
7	Peptide 6	H-Glu-Glu-Lys(N_3)-Ser-Gly-Ser-Thr-Ser-Phe-R8*-Glu-Tyr-Trp-Ala-Leu-Leu-S5*-NH_2
8	Peptide 8	H-Lys(N_3)-betaAla-Leu-Thr-Phe-R8*-Glu-Tyr-Trp-Ala-Gln-Cba-S5*-Ser-Ala-Ala-Lys(mPEG24)-NH_2
9	Peptide 9	Ac-Leu-Thr-Phe-Glu-Glu-Tyr-Trp-Ala-Gln-Leu-Thr-Ser-NH_2

SEQ ID NO.	Peptide Name	Sequence
10	Peptide 10	Ac-DLeu-Thr-Phe-Glu-Glu-Tyr-Trp-Ala-Gln-Leu-Thr-Ser-NH_2
11	Peptide 11	Ac-Leu-Thr-Phe-Aib-Glu-Tyr-Trp-Gln-Leu-Cba-Aib-Ser-Ala-Ala-OH
12	Peptide 12	Ac-Leu-Thr-Phe-Glu-Glu-Tyr-Trp-Ala-DGln-Leu-Thr-Ser-NH_2
13	Peptide 13	H-DThr-DAla-DTrp-DTyr-DAla-DAsn-DPhe-DGlu-DLys-DLeu-DLeu-DArg-NH_2
14	Peptide 14	Ac-DThr-DAla-DTrp-DTyr-DAla-DAsn-DPhe-DGlu-DLys-DLeu-DLeu-DArg-NH_2
15	Peptide 15	Ac-Thr-Ser-(α-Me-Phe)-R8*-Glu-Tyr-Trp-Ala-Leu-Leu-S5*-NH_2
16	Peptide 16	H-DThr-DAla-DTrp(6-F)-DTyr-DAla-DAsn-DPhe(4-CF3)-DGlu-S5*-DLeu-DLeu-R5*-NH_2
17	Peptide 17	Ac-Leu-Thr-DPhe-R8*-Glu-Tyr-Trp-Ala-Gln-Leu-S5*-Ala-Ala-Ala-Ala-Ala-DAla-NH_2
* = site of stapling; S5 = (S)-2-(4'-pentenyl) alanine; R8 = (R)-2-(7'octenyl) alanine; Aib = 2-aminoisobutyric acid; mPEG24 = mono methylated polyethylene glycol; E8 = (S)-2-(7'octenyl) alanine; R5 = (R)-2-(4'-pentenyl) alanine; B5 = 2-amino-2-(pent-4-enyl)hept-6-enoic acid; Cba = cyclobutyl alanine; D-amino acids = DAaa		

[0086] The inventors measured p53 activation at 10 μM of each peptide and observed that the peptides generally fall into three groups: (i) peptides whose activities are unchanged by DμVS processing, (ii) peptides that show enhanced activity with DμVS-processed cells, and (iii) peptides that show no activity in either format (FIG. 5A). The control peptides behaved as expected – Peptide 1 displayed no difference in activity, Peptide 2 showed improved activity following DμVS, and the non-binding Peptide 17 had activity that was unaffected by DμVS. Of the remaining thirteen peptides, only three had enhanced activity in the p53 reporter assay when the cells were processed in the DμVS system (in addition to Peptide 2; FIG. 5A). These activities were confirmed through dose-response experiments where low micromolar potency was observed (FIGS. 5B-5D). Nine peptides showed no cell-based activity even in the permeabilized cell format, despite several of them binding to MDM2 with KDs in the nanomolar range (FIG. 5A). These data suggest that binding to MDM2 is not sufficient for p53 activation. This

underscores how the DμVS technique can improve understanding of complex modalities, such as cyclic peptides, and intracellular target engagement.

[0087] While several peptides in the "impermeable" group did show a low level of activity at 30 μM, this is a relatively high concentration for in vitro cell-based screening and dose-dependent activity confirmation would be unattainable. In contrast, DμVS significantly left-shifted those dose response curves to confirm bona fide functional target engagement, suggesting that such peptides would be good candidates for chemistry-based permeability optimization.

[0088] Importantly, the inventors also identified potent biochemical binders which have no cellular activity even with DμVS; identification of these sort of true negatives would be valuable information in an SAR effort. The peptides whose functional activities were improved by DμVS seemed to be skewed toward those with better binding affinities, which would seem to agree with current opinion on a key molecular property of a functional peptide being a very high affinity binder (K_D < 10 nM) (Sawyer et al., 2018). However, this was not always the case as Peptide 8 showed functional activity (DμVS-p53 reporter EC_{50} = 1.4 μM, MDM2 binding K_D = 117 nM) and MP-3313 was a very high-affinity peptide that showed no activity improvement (DμVS-p53 reporter EC_{50} > 30 μM, MDM2 binding K_D = 1.7 nM). While the data set is limited, the throughput of the DμVS platform has the ability to provide data that would help to resolve such characteristics in the future.

Example 6: Minimal pressure to run system

[0089] The flow rate at various pressures was tested with UltraPure Deionized water (10977015; Invitrogen; Carlsbad CA) to find the minimum pressure needed to induce fluid flow using a μVS mechanoporation device in this example. The water was connected to the 15 ml P-CAP of the DμVS system, and 2 ml were used to prime the system. 100 μl of water was dispensed into 2 columns of a 96-well plate (Costar 3915; Corning Inc., Corning NY) at 120 psi and the flow rate was recorded. After the columns were filled, the pressure was decreased and the water dispense was performed again, and this was repeated until failure of fluid flow. The data points recorded during these dispense cycles were plotted according to the pressure the system was operating at (FIG. 6). The data was analyzed using GRAPHPAD PRISM®.

Example 7: Pressure dependent cell death with DμVS

[0090] HeLa cells were maintained as described above. The cells were resuspended in Dulbecco's Modified Eagle Medium (10569-010, Gibco) with 10% fetal bovine serum (FBS, Gibco 10082-139), and antibiotics (penicillin (100 units/ml) and 1% streptomycin (100 μg/ml),

Gibco 15140-122) to a density of 250,000 cells/mL using the Vi-Cell XR (383674BA; Beckman Coulter Life Sciences; Brea, CA). The suspension was connected to the 15 ml P-CAP of the DμVS system, and 2 ml were used to prime the system. 100 μl of cells were dispensed into 3 columns of a 96-well plate (Costar 3915; Corning Inc., Corning NY) at 30 psi. This was repeated at 60 psi and 120 psi, and then 100 μl of cells were manually plated into 3 columns (0 psi). The plate was incubated in 5% CO_2 at 37°C for 6 hours. After incubation, Cytotox Green Dye (4633; Sartorius; Göttingen, Germany) was dispensed to each well with an HP D300E digital dispenser to a final concentration of 250 nM. The plate was incubated in 5% CO_2 at 37°C for 30 minutes in the Incucyte S3 (9600-0031; Sartorius; Göttingen, Germany) and then imaged. The resulting data was plotted as green fluorescence signal (cytotoxicity), normalized to the confluence of cells (relative cell number) for each applied pressure (FIG. 7). The data was analyzed using GRAPHPAD PRISM®.

METHODS

Delivery of fluorescently labeled 3kD dextran into HeLa and HCT116 cells

[0091] The human cell lines HeLa and HCT116 were purchased from American Type Culture Collection (ATCC, Manassas, VA, USA). HeLa cells were maintained in Dulbecco's Modified Eagle Medium (10569-010, Gibco) with 10% fetal bovine serum (FBS, Gibco 10082-139), and antibiotics (penicillin (100 units/ml) and streptomycin (100 μg/ml), Gibco 15140-122) in 5% CO2 at 37 °C. HCT116 cells were maintained in McCoy's 5 A Medium (ATCC, 30–2007) with 10% FBS, and antibiotics (penicillin 100 units/ml, and streptomycin 100 μg/ml), in 5% CO_2 at 37°C. AlexaFluor-488 dextran (AF488-dextran, 3 kDa MW) was purchased from Invitrogen (D34682).

[0092] AF488-dextran was delivered to cells using the HYDROPORE™ microfluidic vortex shedding (μVS) system with 40 μm inline-filter devices from Indee Labs (Berkeley, CA, USA; Jarrell et al. 2019). Cells (HeLa or HCT116) were suspended at 3 x 10^6 cells/ml in 0.2-μm filtered PBS with 3% FBS (v/v) in 1.5 ml Eppendorf BIOPUR™ tubes (05-402-24B, Fisher Scientific). AF-488-dextran was added at 0.2 mg/ml at a final volume of 0.5 ml. For "post-mixed" samples, 0.45 ml of cells in buffer were in the Eppendorf tube and 50 μl of AF-488-dextran (or buffer vehicle) were added to the bottom of 15 ml conical collection tubes. Eppendorf tubes were connected to μVS system with an Elveflow microfluidic reservoir adaptor (LVF-KPT-XS-2_2, Darwin Microfluidics, France). Samples were processed at 120 psi and received in the collection tube. After μVS processing, cells were pelleted by centrifugation (300 x g, 5 min), and the buffer with excess AF-488-dextran was removed and discarded. Media with FBS was

added and the cells were incubated at 37 °C, 5% CO_2 for 1.5 h. After incubation, cells were washed, labeled with LIVE/DEAD™ Fixable Yellow Dead Cell Stain Kit (L34959, Invitrogen) according to the manufacturer's protocol, and analyzed via flow cytometry.

[0093] For the kinetic analysis of membrane resealing, the zero time point samples were processed as described above for "post-mixed" samples. For subsequent time points, the suspension was passed through the μVS system in bulk from a 15 ml Falcon tube with a P-CAP metal reservoir cap (Fluigent; Le Kremlin-Bicêtre, France) and added to AF-488-dextran at pre-determined timepoints (1, 2, 4, 8, 16 and 32 min). Cells were then processed and analyzed as described above. Data represent mean and standard deviation among at least two replicates. Data were plotted in GRAPHPAD PRISM® and a one phase decay model was used to fit a curve to the data.

Setup and characterization of DμVS system

[0094] An N_2 tank (N5.0, cylinder size 300, Middlesex Gases, Everett MA, USA) supplied air through 1/8" OD FEP tubing to an electronic pressure regulator (VEAA-L-3-D11-Q4-V1-1R1; Festo Corp., Islandia NY). Using 0-10 VDC command, the proportional-pressure regulator provided indicated head-pressure to a 15 ml Falcon tube with a P-CAP metal reservoir cap. Liquid was flowed from the reservoir tube through 1.5 mm OD PTFE tubing through a liquid flow sensor (SLF3S-1300F; Sensirion AG, Switzerland) to a HYDROPORE™ μVS system containing a 40 μm inline-filter device. Upon leaving the device, fluid/cell suspension traveled to a high-speed 2-way axial flow microsolenoid valve (INKX0514300A A; The Lee Company, Westbrook CT) and exited through a 0.01" ID dispense nozzle (INZA5100914K A; The Lee Company, Westbrook CT) onto a microplate of standard SBS footprint of the user's choosing. Microplates that could be used include custom grid labware that can also be defined with a maximum density of 384 positions. The microplate was situated in a 3D-printed holder stationed on a planar surface gantry (EXCM-30; Festo Corp., Islandia NY). The dispense valve and tip were mounted onto a spindle axis (ELGC-BS-KF-45-200-10P; Festo Corp., Islandia NY), which lowers the tip in the z-direction to a configurable height above the microplate when the DμVS program is activated.

[0095] The DμVS process was coordinated by an automation software, Telios, which was developed in-house using LabVIEW programming (National Instruments, Austin, TX; Cassaday et al., 2017; Squadroni et al., 2022). Users wrote a plate map in a .csv file, indicating the plate layout and desired volume filled per well. Once uploaded, the user selected the desired pressure for an experimental run, as well as the system prime volume (optional). The user would load a

new μVS device into the chip housing unit, place the desired microplate onto the X-Y-Z motorized stage, and connect a cell suspension or cell-free solution to the P-CAP. Once these were ready, the user initiated the DμVS program. The software sent a command to close the dispense valve, followed by a command to the pressure regulator to initiate pressure. Next, Telios sent a command to the x-y stage to move the plate to the desired location relative to the dispense tip and to lower the dispense tip to the configured height (typically a few millimeters above microplate). Once the dispense tip and plate were in position, a command was sent to open the valve. Due to the applied pressure, cells or solution were pneumatically pushed through the system and the flow sensor sent a running count of the displaced volume in the DμVS system every 20 ms. Once the target volume was achieved, Telios commanded the valve to close, followed by a command to move the plate to the next desired location, and then another command to re-open the valve. This process was repeated until the uploaded plate map was completed. At completion, the valve was closed, dispense tip was returned to resting z-height, and the filled microplate was returned to the home position.

[0096] μVS devices were discarded after usage with every plate. The dead volume of the tubing and parts downstream of the μVS device was ~200 μl. Therefore, this was the volume that had to be displaced before mechanoporated cells were delivered to their respective payload. While the flow rate of the DμVS system at 120 psi was ~8 ml/min, this flow rate was frequently interrupted by the valve closing during the time that it takes to move a plate. Therefore, the residence time required for cells to clear the dead volume was dependent on flow rate, volume dispensed per well, and plate format (move time between wells). Within this work, the residence time ranged from ~2.8 sec (dispensing 100 μl on 96-well plate) to as long as ~8.5 sec (dispensing 20 μl on 384-well plate).

[0097] For characterization of uniformity of dispensing volumetric fluid, fluorescein isothiocyanate-dextran (average molecular weight 20,000; FD20, Sigma-Aldrich, Waltham MA) was used as a fluorescent tracer. FD20 was solubilized at 0.1 μg/ml in PBS and 0.2 μm-filtered. A reservoir of FD20 was connected to the DμVS system and processed at 120 psi. The dispense volume was set at 50 μl for a 96-well plate (Costar 3915; Corning Inc., Corning NY) and 20 μl for a 384-well plate (Corning 3764; Corning Inc., Corning NY). An equivalent volume of PBS was pre-filled on the plate to mimic the conditions at which the cell-based assays described below were performed. For characterizing uniformity of cell suspension dispensing, HeLa cells were resuspended in 0.2 μm-filtered PBS at 200,000 cells/ml and labeled with 10 μM CELLTRACKER™ Red CMTPX Dye (C34552; Invitrogen, Waltham MA). Similar to the volumetric characterization, cells were DμVS-processed at 120 psi and dispensed at 50 μl or 20

µl (for 96- and 384-well plates, respectively) into wells that were pre-filled with an equivalent volume of PBS. All wells were filled with FD20 or CELLTRACKER™-labeled HeLa cells except for three wells on a 96-well plate and six wells on a 384-well plate, to serve as background controls. After dispensing, fluorescence was measured on a PHERASTAR® FSX microplate reader (BMG Labtech, Ortenberg, Germany).

NANOCLICK™ permeability assay

[0098] NANOBRET® 618-azide (NB618Az), DIBAC-chloroalkane (DIBAC-CA), and Intracellular TE NANO-GLO® Substrate/Inhibitor (N2160) were purchased from Promega Corp., Madison WI. Assay-ready frozen (ARF) HeLa NANOCLICK™ cells were prepared as previously described (Peier et al., 2021). Cells were thawed, resuspended in Opti-MEM (11058-021, Invitrogen, Waltham MA) with 1% v/v FBS, and allowed to incubate overnight on 150 mm tissue culture plates (Corning 430599; Corning Inc., Corning NY). Peptides were synthesized as previously described (Partridge et al., 2019; Peier et al., 2021). To set up the assay, peptides were pre-plated in 50 µl Opti-MEM on opaque white 96-well plates (Corning 3917; Corning Inc., Corning NY) using a HP D300E digital dispenser. Maximum DMSO concentration used was 0.3% v/v. After overnight incubation, media was removed and replaced with 3 µM DIBAC-CA in Opti-MEM with 1% v/v FBS. Cells were incubated for 1 h with DIBAC-CA at 37 C, then washed twice with PBS and treated with 0.05% v/v trypsin to lift cells. Cells were spun down for 5 min at 300 x g, resuspended in Opti-MEM (without FBS), 70-µm strained (130-098-462; Miltenyi Biotec, Bergisch Gladbach, North Rhine-Westphalia, Germany) and then brought to a final cell density of 2 x 10^5 cells/ml in PBS. Cell suspension was connected to the 15 ml P-CAP of the DµVS system, and 2 ml were used to prime the system. The DµVS process was then initiated at 120 psi and 50 µl were dispensed to a microplate containing Opti-MEM with peptides according to predefined plate map in the Telios software. Unprocessed cells and cells treated with digitonin (50 µg/ml; Sigma-Aldrich D141; Burlington, MA) were added to separate 96-well plates in parallel. After DµVS processing/mixing with peptide, cells were spun down for 1 min at 100 x g and then incubated at 37°C with 5% CO2 for 4 h. NB618Az was diluted to 40 µM in Opti-MEM, and 33 µl was added to each well, yielding a final concentration of 10 µM. After a 1 h incubation (37 °C, 5% CO2), 50 µl of a NANOBRET® NANO-GLO® Substrate and extracellular NANOLUC® Inhibitor solution (6 µl substrate, 2 µl inhibitor per 1 ml of Opti-MEM) was added to each well, and the microplate was read on a PHERASTAR® FSX microplate reader (BMG Labtech, Ortenberg, Germany) immediately. NANOBRET® ratio (FIGS. 3A-3H)

was calculated using the sample value (S) and the average of the vehicle controls for each respective processing condition ($mean_{veh}$):

$$NanoBRET\ ratio = \frac{S}{mean_{veh}}$$

EC_{50} values were calculated using the three parameter inhibitor versus response method in GRAPHPAD PRISM®. Dose response experiments were performed with triplicates on plate and repeated at least three separate times. The plate-wide single concentration experiments with 32 on-plate replicates were performed twice independently.

HCT116 p53 β-lactamase reporter gene functional assay

[0099] The CELLSENSOR™ p53RE-*bla* HCT116 cell line (K1640; Thermo Scientific, Waltham, MA) was used for functional characterization of p53 pathway activation by DμVS-delivered peptides. Assay was performed similarly to how previously described (Partridge et al., 2019). These cells harbor a stable integration of a β-lactamase reporter gene under control of the p53 response element. Cells were maintained in McCoy's 5A medium (16600-082; Invitrogen, Waltham MA) with 10% dialyzed FBS (26400-036; Invitrogen, Waltham MA), blasticidin (R210-01, Invitrogen), and penicillin/streptomycin according to the manufacturer's protocol. Peptides were synthesized as previously described (Partridge et al., 2019; Peier et al., 2021). To set up the assay, peptides were first pre-plated in assay medium (Opti-MEM supplemented with 0.1 mM non-essential amino acids [11140-050; Invitrogen, Waltham, MA], 1 mM sodium pyruvate [11360-070; Invitrogen, Waltham MA], and penicillin/streptomycin) without FBS on 384-well plates (Corning 3764; Corning Inc., Corning NY) or 96-well plates (Corning 3603; Corning Inc., Corning NY) using a HP D300E digital dispenser (20 μl 384-well, 50 μl 96-well). Maximum DMSO concentration used was 0.3% v/v. Cells were washed, resuspended with 0.05% v/v trypsin, spun down for 5 min at 300 x g, and resuspended in PBS. Cells were 70-μm strained and then brought to a final cell density of 3 x 106 cells/ml in PBS. Cell suspension was connected to 15 ml P-CAP of the DμVS system, and 2 ml were used to prime the system. DμVS process was then initiated at 120 psi and 20 μl (384-well) or 50 μl (96-well) were dispensed to microplate in wells that were pre-defined in the Telios software and pre-loaded with peptides 2X in assay medium. Unprocessed cells were added to the microplate in parallel. After DμVS processing/mixing with peptide, cells were incubated at 37 °C for 4 h. β-lactamase activity was detected using the TOXBLAZER™ loading kit (K1095; Invitrogen, Waltham MA) according to the manufacturer's protocol. Plates were measured using the PHERASTAR™ FSX microplate reader with a LIVEBLAZER™ optic module (1400-G3M-FI-410-530-460, BMG Labtech;

Ortenburg, Germany). Maximum p53 activity was defined as the β-lactamase activity induced by 30 μM Peptide 1 ($mean_{pos}$). Percent activation of individual samples (S) was calculated using the following equation, where $mean_{veh}$ represents the mean of vehicle controls:

$$\%\ activation = \frac{S - mean_{veh}}{mean_{pos} - mean_{veh}} * 100$$

Z-factors were calculated using the formula:

$$Z' = 1 - \frac{3\sigma_{pos} + 3\sigma_{veh}}{|mean_{pos} - mean_{veh}|}$$

$Mean_{pos}$ and σ_{pos} represent the mean and standard deviation, respectively, of the raw ratiometric values for 30 μM Peptide 1 and $mean_{veh}$ and σ_{veh} represent the mean and standard deviation of the vehicle controls. Dose-response data EC_{50} values were determined using the "[Agonist] vs. response – Variable slope (four parameters)" algorithm in GRAPHPAD PRISM®. Single concentration data for expanded peptide set were analyzed using unpaired T-tests with False Discovery Rate (FDR, 1.00%) multiple comparisons correction using the two-stage step-up (Benjamini, Krieger, and Yekutieli) method. Data were accumulated from at least five independent experimental runs.

MDM2 Binding Assay

[0100] MDM2 protein generation and binding studies were performed as described (Partridge et al., 2019). Briefly, binding was performed using MDM2 (1–125) protein (Genbank Accession AAL13243; MCNTNMSVPTDGAVTTSQIPASEQETLVRPKPLLLKLLKSVGAQKDTYTMKEVLFYLGQ YIMTKRLYDEKQQHIVYCSNDLLGDLFGVPSFSVKEHRKIYTMIYRNLVVVNQQESSDS GTSVSEN; SEQ ID NO: 18) titrated against 50 nM carboxyfluorescein (FAM)-labeled 12/1 peptide13 (FAM-RFMDYWEGL-NH2; SEQ ID NO: 19). The apparent K_D value of FAM-labeled 12/1peptide was determined to be 13.0 nM and subsequently used to determine the apparent K_D values of the respective competing ligands in competition assays in fluorescence anisotropy experiments. Titrations were carried out with the concentration of MDM2 held constant at 250 nM and the labeled peptide at 50 nM. The competing molecules were then titrated against the complex of the FAM-labeled peptide and protein. Curve-fitting was carried out using Prism 4.0 (GraphPad, Boston MA) to determine K_D values. Readings were carried out with an Envision Multilabel Reader (PerkinElmer, Waltham, MA). Experiments were carried out

in PBS (2.7 mM KCl, 137mM NaCl, 10 mM Na_2HPO4, and 2 mM KH_2PO_4 (pH 7.4)) and 0.1% Tween 20 buffer. All titrations were carried out in triplicate.

[0101] The disclosed subject matter is not to be limited in scope by the specific embodiments and examples described herein. Indeed, various modifications of the disclosure in addition to those described will become apparent to those skilled in the art from the foregoing description and accompanying figures. Such modifications are intended to fall within the scope of the appended claims.

[0102] All references (*e.g.*, publications or patents or patent applications) cited herein are incorporated herein by reference in their entirety and for all purposes to the same extent as if each individual reference (*e.g.*, publication or patent or patent application) was specifically and individually indicated to be incorporated by reference in its entirety for all purposes. Other embodiments are within the accompanying claims.

References

[0103] Bashiruddin, N. K., and Suga, H. (2015). Construction and screening of vast libraries of natural product-like macrocyclic peptides using in vitro display technologies. Curr. Opin. Chem. Biol. 24, 131–138. doi: 10.1016/j.cbpa.2014.11.011.

[0104] Békés, M., Langley, D. R., and Crews, C. M. (2022). PROTAC targeted protein degraders: the past is prologue. Nat. Rev. Drug Discov. 21, 181–200. doi: 10.1038/s41573-021-00371-6.

[0105] Brown, C. J., Quah, S. T., Jong, J., Goh, A. M., Chiam, P. C., Khoo, K. H., et al. (2013). Stapled peptides with improved potency and specificity that activate p53. ACS Chem. Biol. 8, 506–512. doi: 10.1021/cb3005148.

[0106] Buyanova, M., and Pei, D. (2022). Targeting intracellular protein – protein interactions with macrocyclic peptides. Trends Pharmacol. Sci. 43, 234–248. doi: 10.1016/j.tips.2021.11.008.

[0107] Cassaday, J., Finley, M., Squadroni, B., Jezequel-Sur, S., Rauch, A., Gajera, B., et al. (2017). Development of a Platform to Enable Fully Automated Cross-Titration Experiments. SLAS Technol. 22, 195–205. doi: 10.1177/2211068216679805.

[0108] Chang, Y. S., Graves, B., Guerlavais, V., Tovar, C., Packman, K., To, K. H., et al. (2013). Stapled α-helical peptide drug development: A potent dual inhibitor of MDM2 and MDMX for p53-dependent cancer therapy. Proc. Natl. Acad. Sci. U. S. A. 110. doi: 10.1073/pnas.1303002110.

[0109] DiTommaso, T., Cole, J. M., Cassereau, L., Buggé, J. A., Sikora Hanson, J. L., Bridgen, D. T., et al. (2018). Cell engineering with microfluidic squeezing preserves functionality of primary immune cells in vivo. Proc. Natl. Acad. Sci. U. S. A. 115, E10907–E10914. doi: 10.1073/pnas.1809671115.

[0110] Doty, A. C., Jarvis, C. M., and Munsell, E. V. (2022). "Formulation Strategies to Enable Delivery of Therapeutic Peptides across Cell Membranes," in Approaching the Next Inflection in Peptide Therapeutics: Attaining Cell Permeability and Oral Bioavailability (American Chemical Society), 223–254. doi: 10.1021/bk-2022-1417.ch009.

[0111] Dougherty, P. G., Sahni, A., and Pei, D. (2019). Understanding Cell Penetration of Cyclic Peptides. Chem. Rev. 119, 10241–10287. doi: 10.1021/acs.chemrev.9b00008.

[0112] El-Sayed, M. E. H., Hoffman, A. S., and Stayton, P. S. (2005). Smart polymeric carriers for enhanced intracellular delivery of therapeutic macromolecules. Expert Opin. Biol. Ther. 5, 23–32. doi: 10.1517/14712598.5.1.23.

[0113] Han, X., Liu, Z., Jo, M. C., Zhang, K., Li, Y., Zeng, Z., et al. (2015). CRISPR-Cas9 delivery to hard-to-transfect cells via membrane deformation. Sci. Adv. 1, 1–9. doi: 10.1126/sciadv.1500454.

[0114] Henning, N. J., Boike, L., Spradlin, J. N., Ward, C. C., Liu, G., Zhang, E., et al. (2022). Deubiquitinase-targeting chimeras for targeted protein stabilization. Nat. Chem. Biol. 18, 412–421. doi: 10.1038/s41589-022-00971-2.

[0115] Hochman, J., Sawyer, T., and Duggal, R. (2021). Overcoming Cellular and Systemic Barriers to Design the Next Wave of Peptide Therapeutics. Methods Pharmacol. Toxicol., 201–227. doi: 10.1007/978-1-0716-1250-7_10.

[0116] Hu, B., Gilkes, D. M., and Chen, J. (2007). Efficient p53 activation and apoptosis by simultaneous disruption of binding to MDM2 and MDMX. Cancer Res. 67, 8810–8817. doi: 10.1158/0008-5472.CAN-07-1140.

[0117] Hur, J., and Chung, A. J. (2021). Microfluidic and Nanofluidic Intracellular Delivery. Adv. Sci. 8. doi: 10.1002/advs.202004595.

[0118] Jarrell, J. A., Sytsma, B. J., Wilson, L. H., Pan, F. L., Lau, K. H. W. J., Kirby, G. T. S., et al. (2021). Numerical optimization of microfluidic vortex shedding for genome editing T cells with Cas9. Sci. Rep. 11, 1–13. doi: 10.1038/s41598-021-91307-y.

[0119] Jarrell, J. A., Twite, A. A., Lau, K. H. W. J., Kashani, M. N., Lievano, A. A., Acevedo, J., et al. (2019). Intracellular delivery of mRNA to human primary T cells with microfluidic vortex shedding. Sci. Rep. 9, 1–11. doi: 10.1038/s41598-019-40147-y.

[0120] Jewett, J. C., and Bertozzi, C. R. (2010). Cu-free click cycloaddition reactions in chemical biology. Chem. Soc. Rev. 39, 1272–1279. doi: 10.1039/b901970g.

[0121] Kizer, M. E., Deng, Y., Kang, G., Mikael, P. E., Wang, X., and Chung, A. J. (2019). Hydroporator: A hydrodynamic cell membrane perforator for high-throughput vector-free nanomaterial intracellular delivery and DNA origami biostability evaluation. Lab Chip 19, 1747–1754. doi: 10.1039/c9lc00041k.

[0122] Li, J., Wang, B., Juba, B. M., Vazquez, M., Kortum, S. W., Pierce, B. S., et al. (2017). Microfluidic-Enabled Intracellular Delivery of Membrane Impermeable Inhibitors to Study Target Engagement in Human Primary Cells. ACS Chem. Biol. 12, 2970–2974. doi: 10.1021/acschembio.7b00683.

[0123] Lipinski, C. A., Lombardo, F., Dominy, B. W., and Feeney, P. J. (2001). Experimental and computational approaches to estimate solubility and permeability in drug discovery and development settings. Adv. Drug Deliv. Rev. 46, 3–26. doi: 10.1016/j.addr.2012.09.019.

[0124] Liu, M., Li, C., Pazgier, M., Li, C., Mao, Y., Lv, Y., et al. (2010). D-peptide inhibitors of the p53-MDM2 interaction for targeted molecular therapy of malignant neoplasms. Proc. Natl. Acad. Sci. U. S. A. 107, 14321–14326. doi: 10.1073/pnas.1008930107.

[0125] Los, G. V, Encell, L. P., Mcdougall, M. G., Hartzell, D. D., Karassina, N., Simpson, D., et al. (2008). HaloTag: A Novel Protein Labeling Technology for Cell Imaging and Protein Analysis. ACS Chem. Biol. 3, 373–382.

[0126] Machleidt, T., Woodroofe, C. C., Schwinn, M. K., Méndez, J., Robers, M. B., Zimmerman, K., et al. (2015). NanoBRET-A Novel BRET Platform for the Analysis of Protein-Protein Interactions. ACS Chem. Biol. 10, 1797–1804. doi: 10.1021/acschembio.5b00143.

[0127] Manzari, M. T., Shamay, Y., Kiguchi, H., Rosen, N., Scaltriti, M., and Heller, D. A. (2021). Targeted drug delivery strategies for precision medicines. Nat. Rev. Mater. 6, 351–370. doi: 10.1038/s41578-020-00269-6.

[0128] Moldenhauer, G., Salnikov, A. V., Lüttgau, S., Herr, I., Anderl, J., and Faulstich, H. (2012). Therapeutic potential of amanitin-conjugated anti-epithelial cell adhesion molecule monoclonal antibody against pancreatic carcinoma. J. Natl. Cancer Inst. 104, 622–634. doi: 10.1093/jnci/djs140.

[0129] Morioka, T., Loik, N. D., Hipolito, C. J., Goto, Y., and Suga, H. (2015). Selection-based discovery of macrocyclic peptides for the next generation therapeutics. Curr. Opin. Chem. Biol. 26, 34–41. doi: 10.1016/j.cbpa.2015.01.023.

[0130] Partridge, A. W., Kaan, H. Y. K., Juang, Y. C., Sadruddin, A., Lim, S., Brown, C. J., et al. (2019). Incorporation of putative helix-breaking amino acids in the design of novel stapled

peptides: Exploring biophysical and cellular permeability properties. Molecules 24. doi: 10.3390/molecules24122292.

[0131] Peier, A., Ge, L., Boyer, N., Frost, J., Duggal, R., Biswas, K., et al. (2021). NanoClick: A High Throughput, Target-Agnostic Peptide Cell Permeability Assay. ACS Chem. Biol. 16, 293–309. doi: 10.1021/acschembio.0c00804.

[0132] Phan, J., Li, Z., Kasprzak, A., Li, B., Sebti, S., Guida, W., et al. (2010). Structure-based design of high affinity peptides inhibiting the interaction of p53 with MDM2 and MDMX. J. Biol. Chem. 285, 2174–2183. doi: 10.1074/jbc.M109.073056.

[0133] Philippe, G. J. B., Craik, D. J., and Henriques, S. T. (2021). Converting peptides into drugs targeting intracellular protein–protein interactions. Drug Discov. Today 26, 1521–1531. doi: 10.1016/j.drudis.2021.01.022.

[0134] Qian, Z., Dougherty, P. G., and Pei, D. (2017). Targeting intracellular protein–protein interactions with cell-permeable cyclic peptides. Curr. Opin. Chem. Biol. 38, 80–86. doi: 10.1016/j.cbpa.2017.03.011.

[0135] Renfer, A., Tiwari, M. K., Meyer, F., Brunschwiler, T., Michel, B., and Poulikakos, D. (2013). Vortex shedding from confined micropin arrays. Microfluid. Nanofluidics 15, 231–242. doi: 10.1007/s10404-013-1137-5.

[0136] Sawyer, T. K., Partridge, A. W., Kaan, H. Y. K., Juang, Y. C., Lim, S., Johannes, C., et al. (2018). Macrocyclic α helical peptide therapeutic modality: A perspective of learnings and challenges. Bioorganic Med. Chem. 26, 2807–2815. doi: 10.1016/j.bmc.2018.03.008.

[0137] Sharei, A., Poceviciute, R., Jackson, E. L., Cho, N., Mao, S., Hartoularos, G. C., et al. (2014). Plasma membrane recovery kinetics of a microfluidic intracellular delivery platform. Integr. Biol. (United Kingdom) 6, 470–475. doi: 10.1039/c3ib40215k.

[0138] Sharei, A., Trifonova, R., Jhunjhunwala, S., Hartoularos, G. C., Eyerman, A. T., Lytton-Jean, A., et al. (2015). Ex vivo cytosolic delivery of functional macromolecules to immune cells. PLoS One 10, 1–12. doi: 10.1371/journal.pone.0118803.

[0139] Sharei, A., Zoldan, J., Adamo, A., Sim, W. Y., Cho, N., Jackson, E., et al. (2013). A vector-free microfluidic platform for intracellular delivery. Proc. Natl. Acad. Sci. U. S. A. 110, 2082–2087. doi: 10.1073/pnas.1218705110.

[0140] Solaro, R., Chiellini, F., and Battisti, A. (2010). Targeted delivery of protein drugs by nanocarriers. doi: 10.3390/ma3031928.

[0141] Squadroni, B., Newhard, W., Carr, D., Trinh, H., Racine, F., Zuck, P., et al. (2022). Development of a fully automated platform for agar-based measurement of viable bacterial growth. SLAS Technol. doi: 10.1016/j.slast.2022.03.003.

[0142] Stewart, M. P., Langer, R., and Jensen, K. F. (2018). Intracellular delivery by membrane disruption: Mechanisms, strategies, and concepts. Chem. Rev. 118, 7409–7531. doi: 10.1021/acs.chemrev.7b00678.

[0143] Stewart, M. P., Sharei, A., Ding, X., Sahay, G., Langer, R., and Jensen, K. F. (2016). In vitro and ex vivo strategies for intracellular delivery. Nature 538, 183–192. doi: 10.1038/nature19764.

[0144] Tong, T., Wang, L., You, X., and Wu, J. (2020). Nano and microscale delivery platforms for enhanced oral peptide/protein bioavailability. Biomater. Sci. 8, 5804–5823. doi: 10.1039/d0bm01151g.

[0145] Vinogradov, A. A., Yin, Y., and Suga, H. (2019). Macrocyclic Peptides as Drug Candidates: Recent Progress and Remaining Challenges. J. Am. Chem. Soc. 141, 4167–4181. doi: 10.1021/jacs.8b13178.

[0146] Walport, L. J., Obexer, R., and Suga, H. (2017). Strategies for transitioning macrocyclic peptides to cell-permeable drug leads. Curr. Opin. Biotechnol. 48, 242–250. doi: 10.1016/j.copbio.2017.07.007.

[0147] Zhang, H., and Chen, S. (2022). Cyclic peptide drugs approved in the last two decades (2001-2021). RSC Chem. Biol. 3, 18–31. doi: 10.1039/d1cb00154j.

WHAT IS CLAIMED IS:

1. A system for multiplexed in vitro delivery of exogenous material into at least one cell suspended in a liquid, the system comprising:

a) a microfluidic device having a flow channel configured to disrupt a membrane of the at least one cell and allow the exogenous material to enter the disrupted cell membrane;

b) a sample reservoir in liquid communication with the microfluidic device, the sample reservoir containing a mixture of at least one cell and liquid;

c) a flow sensor positioned between the sample reservoir and the microfluidic device, the flow sensor in liquid communication with the sample reservoir and the microfluidic device;

d) an electronic pressure regulator in gaseous communication with the sample reservoir and a gas supply, wherein the electronic pressure regulator is configured to move the liquid and at least one cell through the flow sensor, into the microfluidic device, and along the flow channel;

e) a dispensing valve in fluid communication with the microfluidic device and in fluid communication with a dispensing tip;

f) an X-Y-Z motorized stage positioned underneath the dispensing tip, the X-Y-Z motorized stage configured to hold a microplate having wells containing liquid and exogenous material; and

g) one or more processors and a memory coupled with the one or more processors, the memory storing instructions which, when executed by the processor, can open and close the dispensing valve and move the X-Y-Z motorized stage, wherein the one or more processors are in data communication with the flow sensor, the electronic pressure regulator, the dispensing valve, and the X-Y-Z motorized stage.

2. The system of claim 1, wherein the flow channel of the microfluidic device includes at least two flow diverters, and the gap between the at least two flow diverters has a width greater than the diameter of the cell.

3. The system of claim 1, wherein the flow channel of the microfluidic device includes at least one cell-deforming constriction wherein the diameter of the constriction is from about 20 to about 60% of the diameter of the cell.

4. A method for multiplexed in vitro delivery of exogenous material into at least one cell suspended in a liquid comprising:

a) adding gaseous pressure to a sample reservoir containing the liquid and the at least one cell;

b) moving a dispensing tip above a first microplate well, wherein the dispensing tip is in liquid communication with a dispensing valve and the dispensing valve is in liquid communication with the sample reservoir;

c) opening the dispensing valve to move the liquid and the at least one cell through a flow sensor due to the gaseous pressure;

d) detecting the flow rate of the liquid, sending detected flow rate data to a processor, and calculating a cumulative flow of the liquid; and

e) closing the dispensing valve when the cumulative flow of the liquid through the flow sensor has reached a volume such that the at least one cell has flowed through a microfluidic device having a flow channel configured to disrupt a membrane of the at least one cell, through the dispensing valve and the dispensing tip, and into the first microplate well containing the exogenous material.

5. The method of claim 4, wherein the flow channel of the microfluidic device includes at least two flow diverters, and the gap between the at least two flow diverters has a width greater than the diameter of the cell.

6. The method of claim 4, wherein the flow channel of the microfluidic device includes at least one cell-deforming constriction wherein the diameter of the constriction is from about 20 to about 60% of the diameter of the cell.

7. The method of any one of claims 4-6, comprising the step of moving the dispensing tip to a second microplate well.

8. The system of any one of claims 1-3 or the method of any one of claims 4-7, wherein the exogenous material is one or more cell-impermeable molecules.

9. The system of any one of claims 1-3 or the method of any one of claims 4-8, wherein the exogenous material is selected from the group consisting of: a composition having one or more active pharmaceutical ingredients; a molecular glue; a deubiquitinase-targeting chimera; a lysosome-targeting chimaera for degradation of extracellular proteins; an autophagy-targeting chimera; an autophagosome-tethering compound; a phosphorylation-targeting chimera; and a ribonuclease targeting chimera degrader.

10. The system of any one of claims 1-3 or the method of any one of claims 4-9, wherein the exogenous material is selected from the group consisting of: an inorganic compound; a drug; a nucleic acid; a plasmid; a protein; a carbohydrate; and a synthetic polymer.

11. The system of any one of claims 1-3 or the method of any one of claims 4-9, wherein the exogenous material is a proteolysis-targeting chimera molecule.

12. The system of any one of claims 1-3 or the method of any one of claims 4-7, wherein the exogenous material is a cyclic peptide.

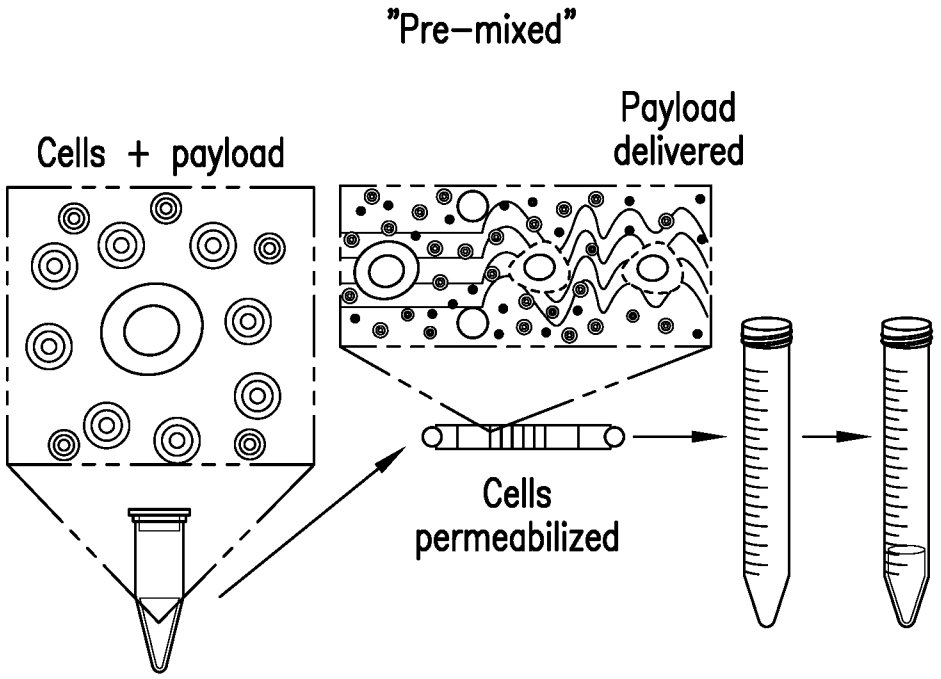
"Pre-mixed"
Cells + payload
Payload delivered
Cells permeabilized

FIG.1A

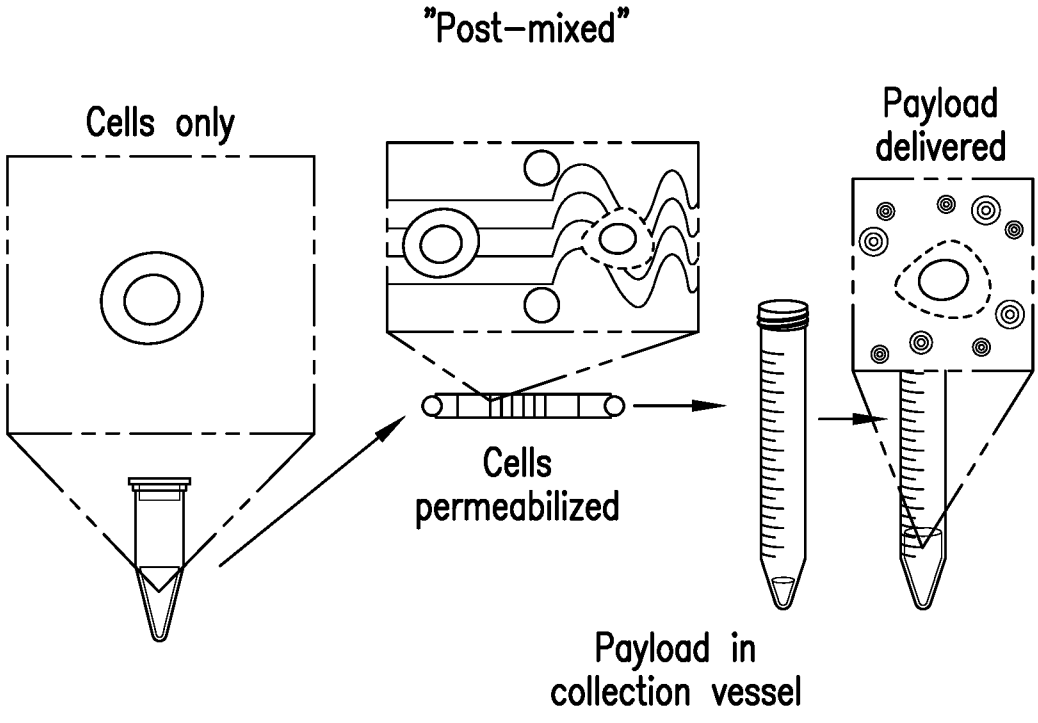
"Post-mixed"
Cells only
Payload delivered
Cells permeabilized
Payload in collection vessel

FIG.1B

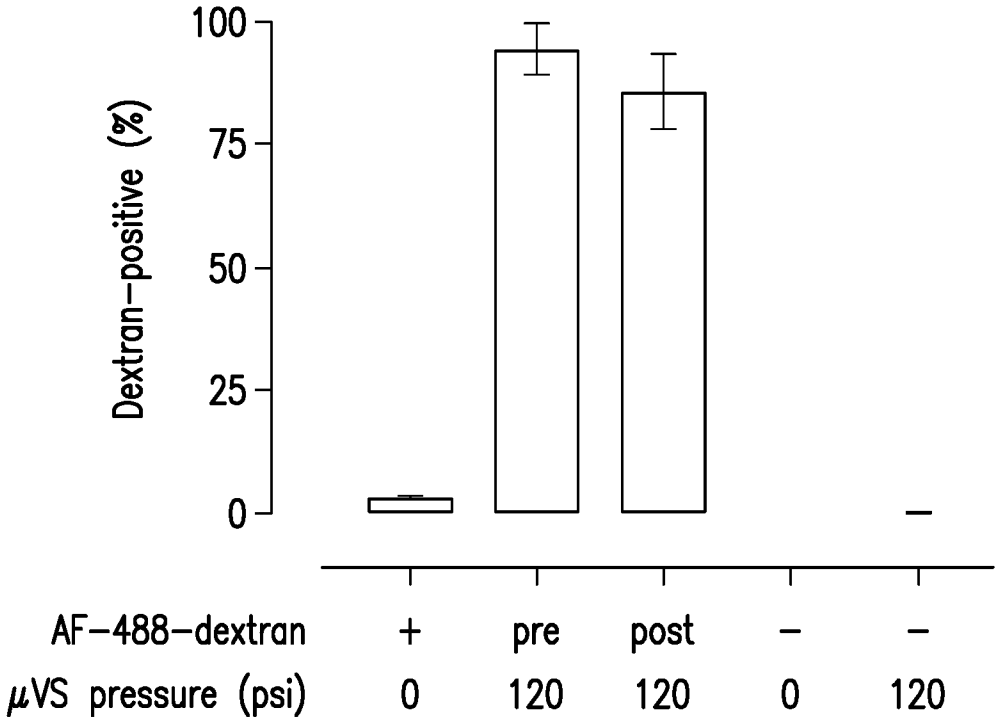
100
75
50
25
0
Dextran−positive (%)
AF−488−dextran + pre post − −
μVS pressure (psi) 0 120 120 0 120

FIG.1C

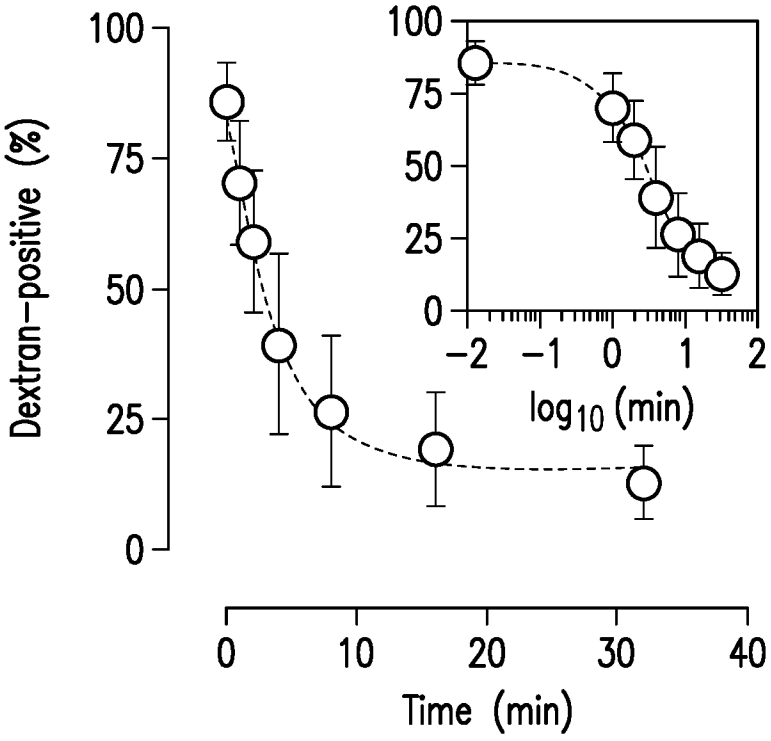
100
75
50
25
0
Dextran−positive (%)
0 10 20 30 40
Time (min)
100
75
50
25
0
−2 −1 0 1 2
log10 (min)

FIG.1D

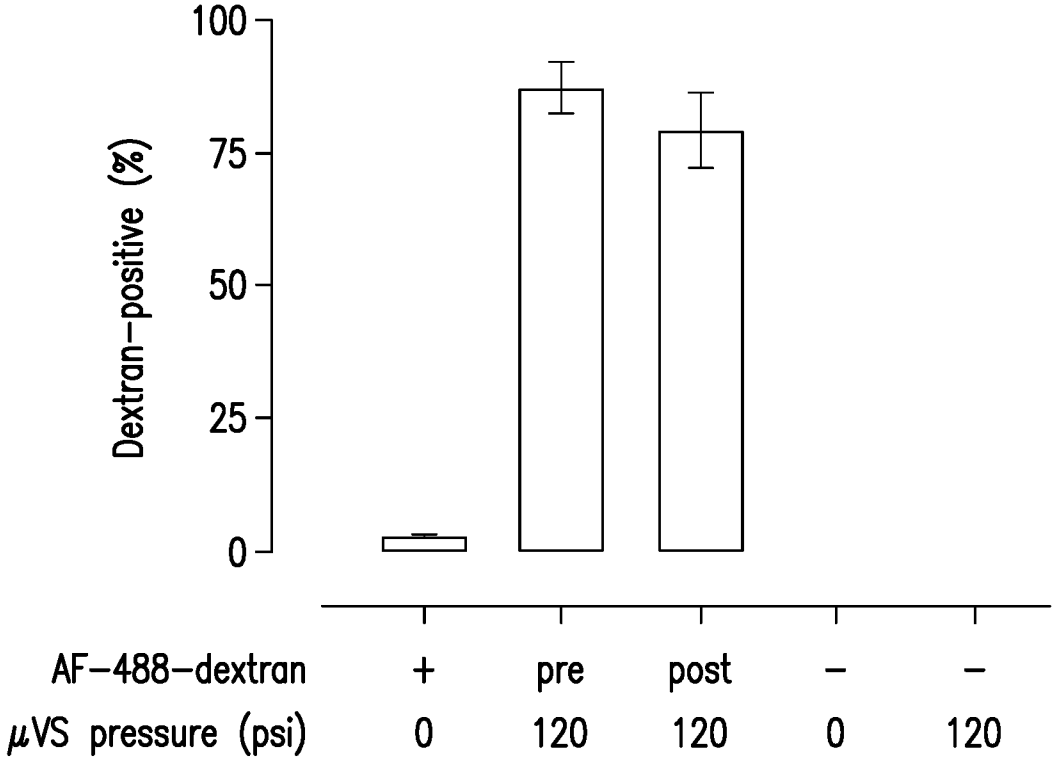
100
75
50
25
0
Dextran−positive (%)
AF−488−dextran + pre post − −
μVS pressure (psi) 0 120 120 0 120

FIG. 1E

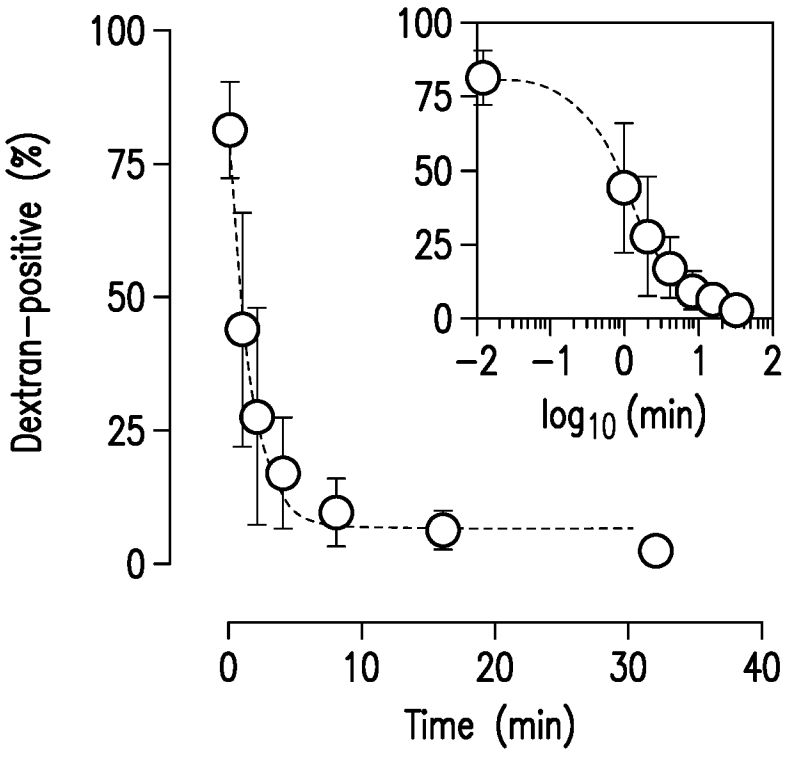
100
75
50
25
0
Dextran−positive (%)
0 10 20 30 40
Time (min)
100
75
50
25
0
−2 −1 0 1 2
log10 (min)

FIG. 1F

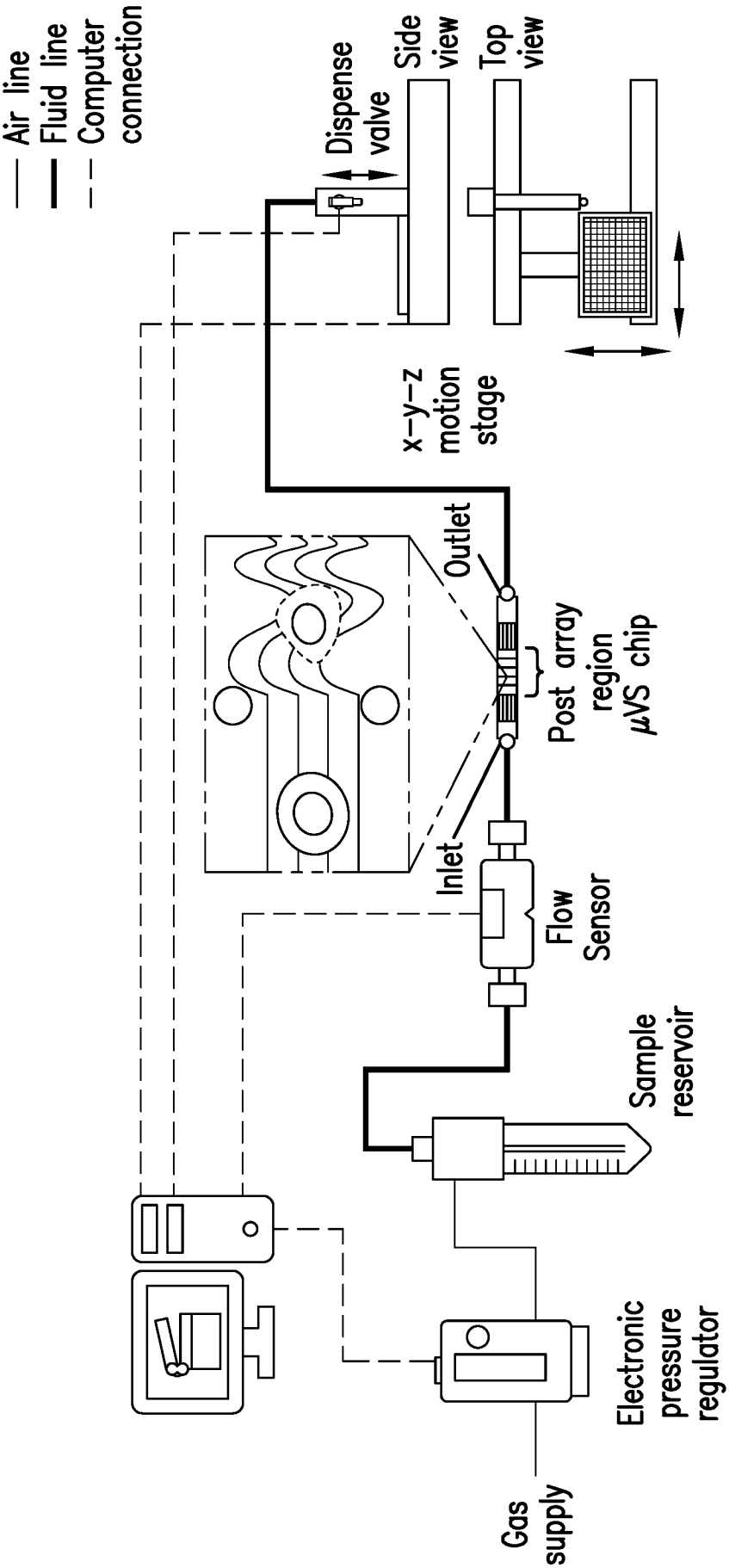
Air line
Fluid line
Computer connection
Dispense valve
Side view
Top view
x–y–z motion stage
Outlet
Post array region
μVS chip
Inlet
Flow Sensor
Sample reservoir
Electronic pressure regulator
Gas supply

FIG.2A

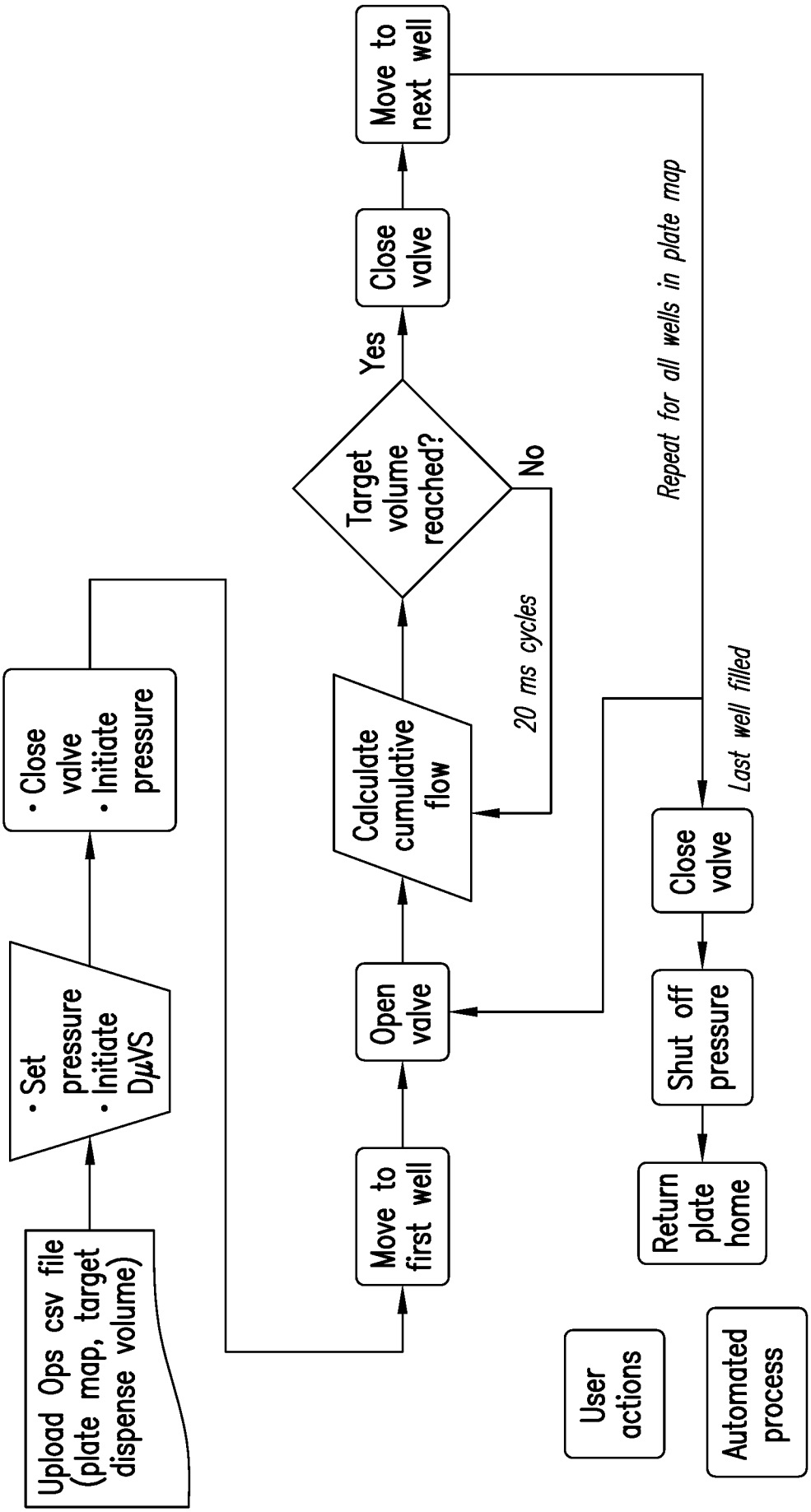
Upload Ops csv file (plate map, target dispense volume)
• Set pressure
• Initiate DμVS
• Close valve
• Initiate pressure
Move to first well
Open valve
Calculate cumulative flow
Target volume reached?
Yes
No
20 ms cycles
Close valve
Move to next well
Repeat for all wells in plate map
Last well filled
Close valve
Shut off pressure
Return plate home
User actions
Automated process

FIG.2B

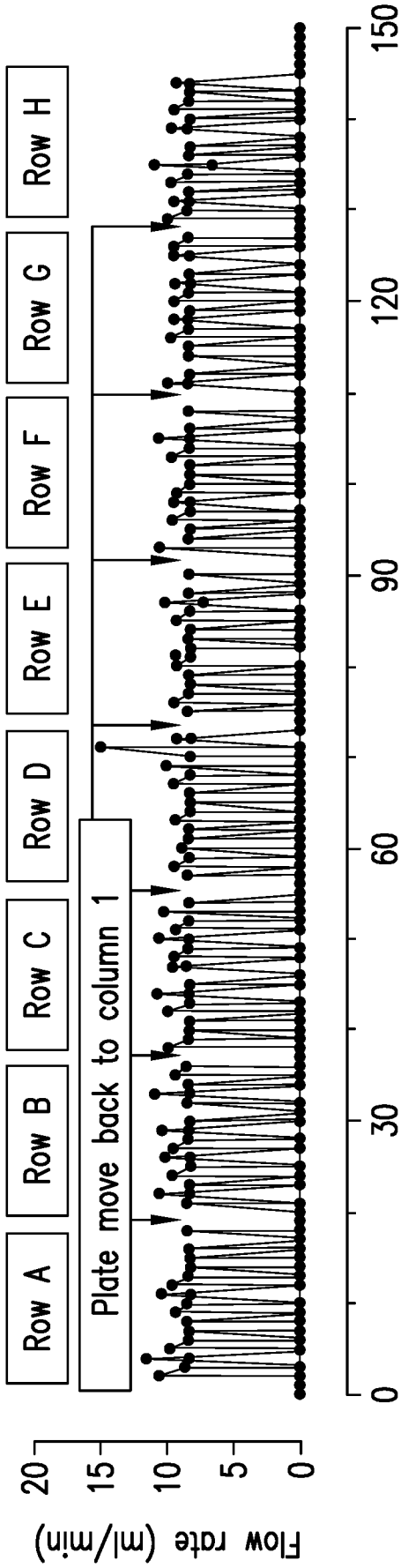
Row A
Row B
Row C
Row D
Row E
Row F
Row G
Row H
Plate move back to column 1
Flow rate (ml/min)
20
15
10
5
0
0
30
60
90
120
150
Time (s)

FIG.2C

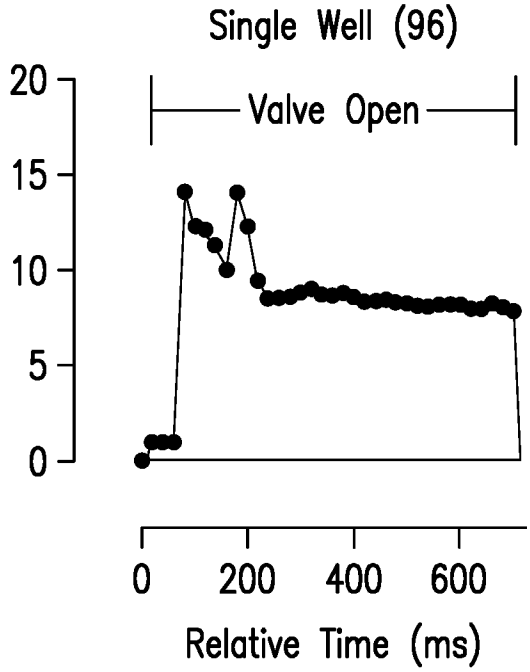
Single Well (96)
Valve Open
20
15
10
5
0
0
200
400
600
Relative Time (ms)

FIG.2D

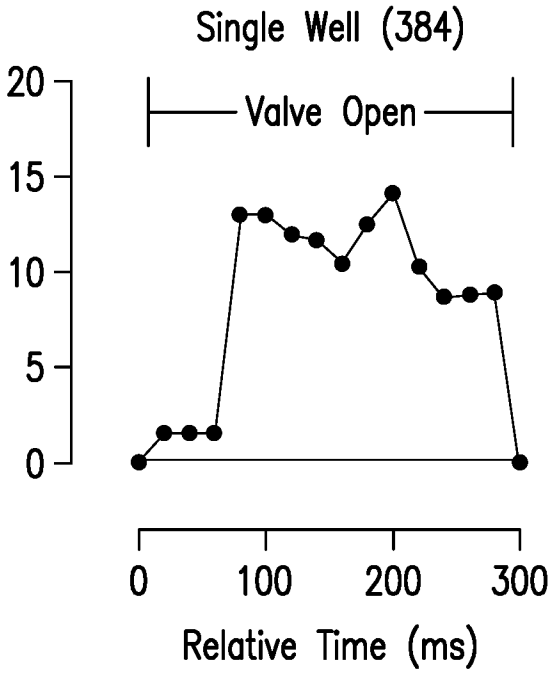
Single Well (384)
Valve Open
20
15
10
5
0
0
100
200
300
Relative Time (ms)

FIG.2E

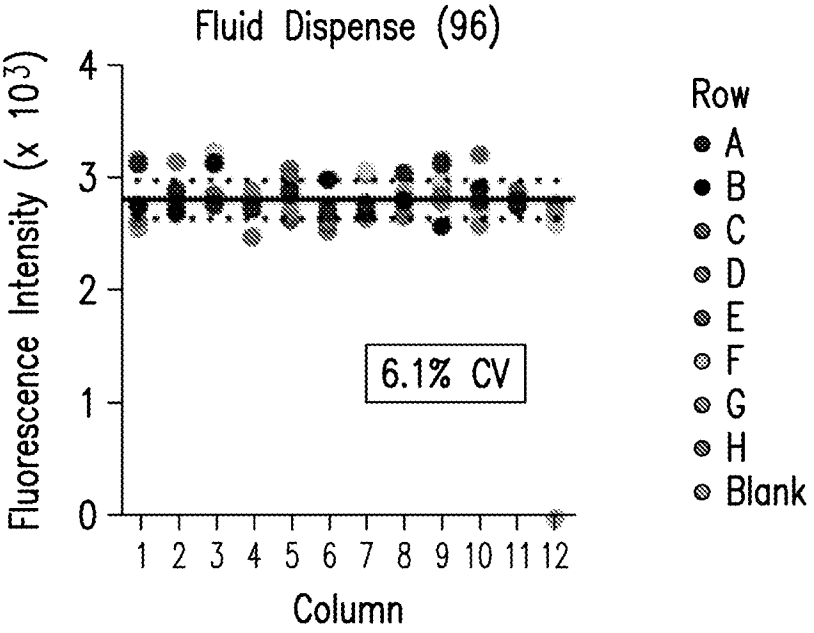
Fluid Dispense (96)
Fluorescence Intensity (x 10^3)
0
1
2
3
4
1 2 3 4 5 6 7 8 9 10 11 12
Column
6.1% CV
Row
A
B
C
D
E
F
G
H
Blank

FIG.2F

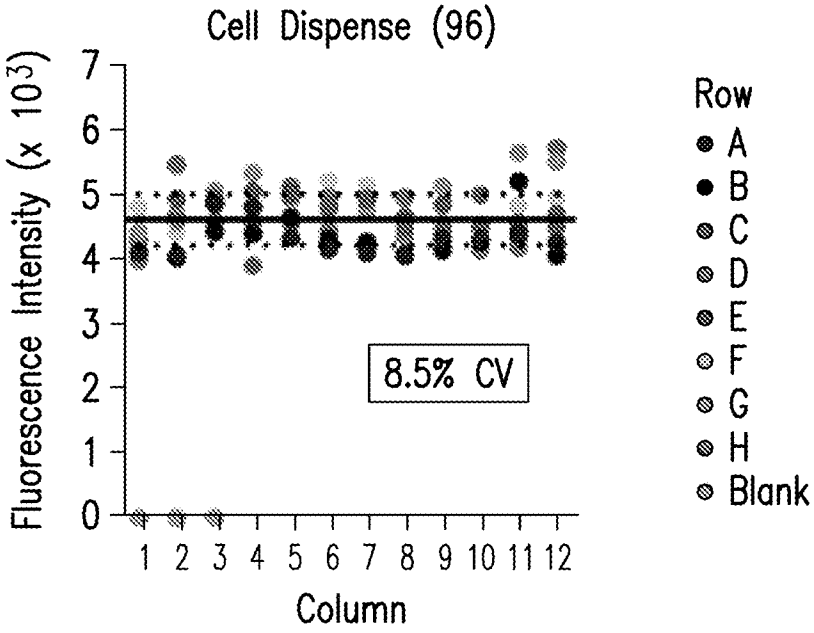
Cell Dispense (96)
Fluorescence Intensity (x 10^3)
0
1
2
3
4
5
6
7
1 2 3 4 5 6 7 8 9 10 11 12
Column
8.5% CV
Row
A
B
C
D
E
F
G
H
Blank

FIG.2G

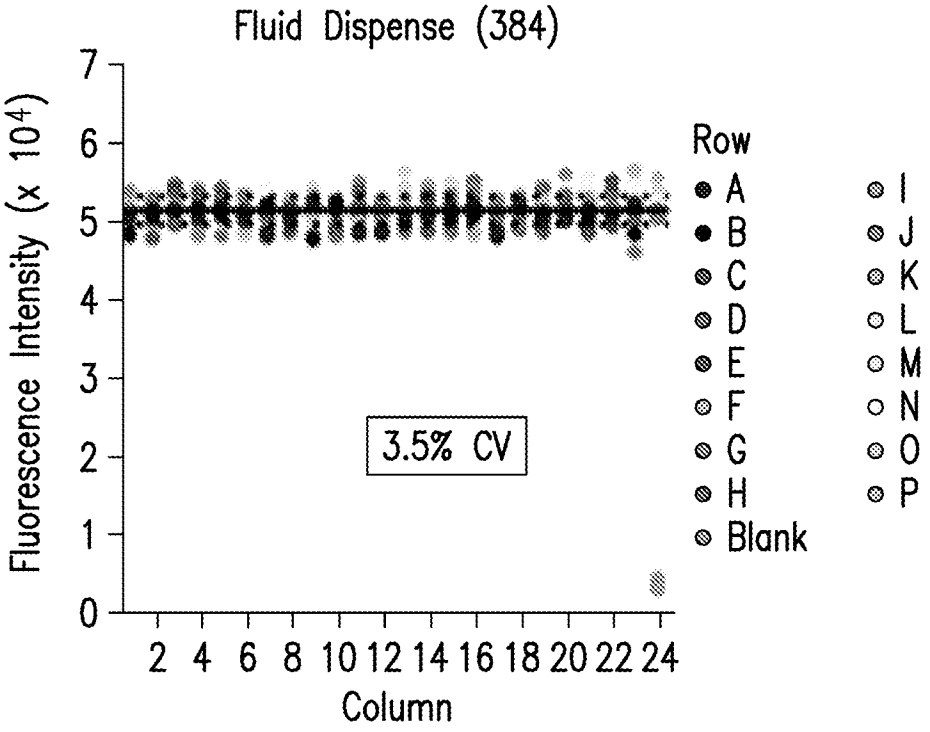
Fluid Dispense (384)
Fluorescence Intensity (x 10⁴)
0
1
2
3
4
5
6
7
2 4 6 8 10 12 14 16 18 20 22 24
Column
3.5% CV
Row
A
B
C
D
E
F
G
H
Blank
I
J
K
L
M
N
O
P

FIG.2H

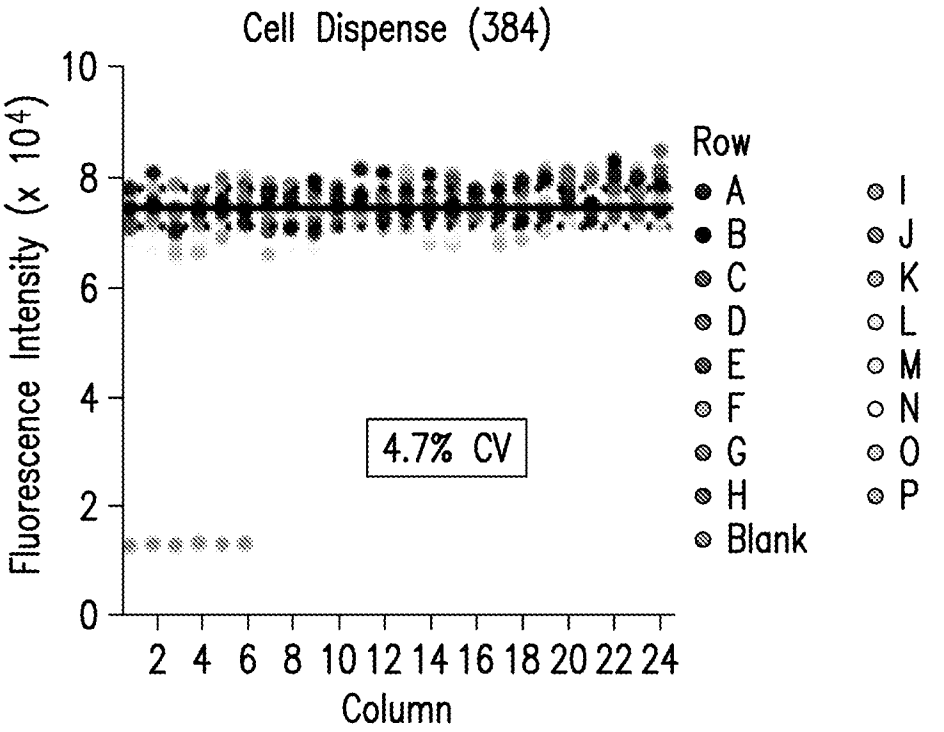
Cell Dispense (384)
Fluorescence Intensity (x 10⁴)
0
2
4
6
8
10
2 4 6 8 10 12 14 16 18 20 22 24
Column
4.7% CV
Row
A
B
C
D
E
F
G
H
Blank
I
J
K
L
M
N
O
P

FIG.2I

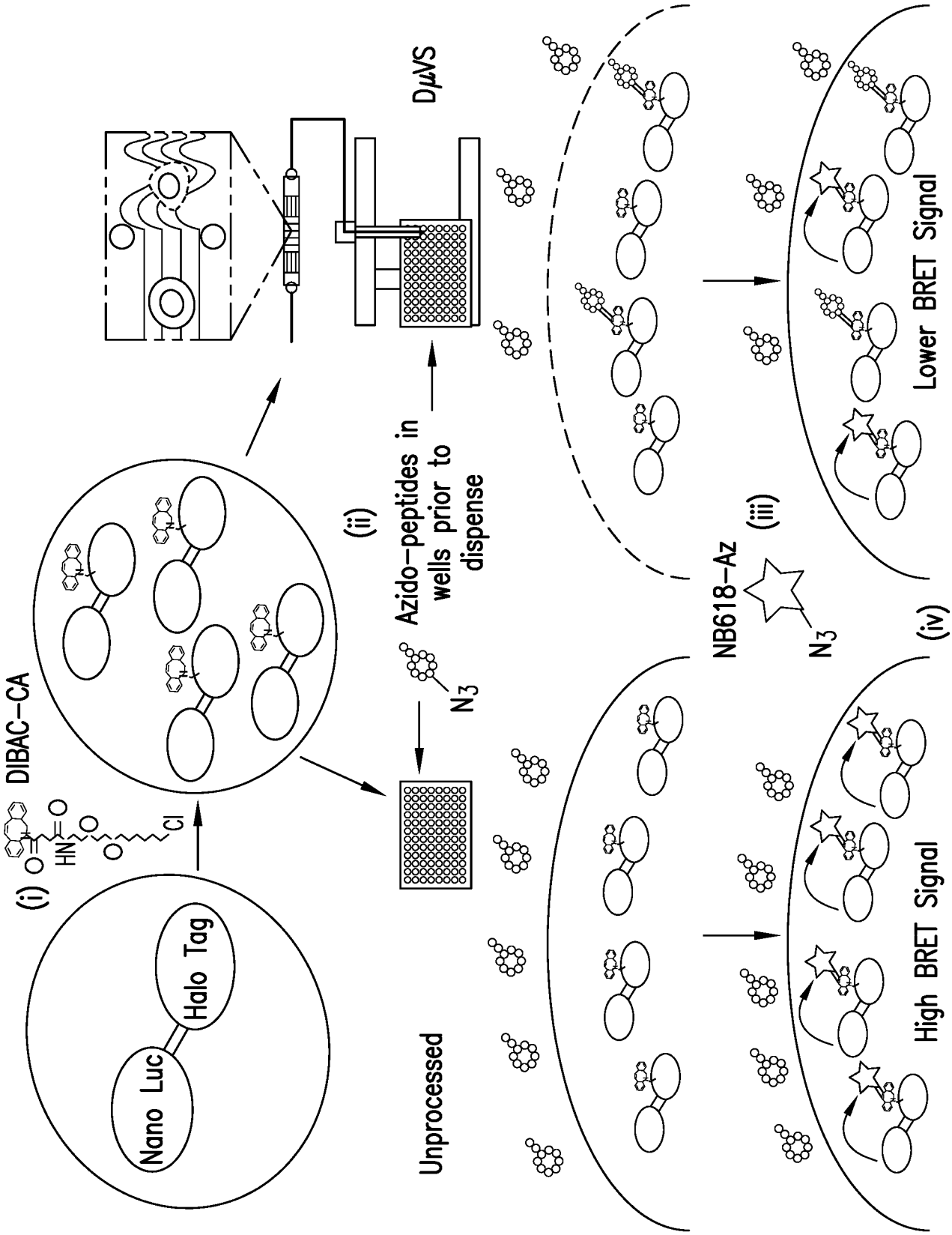
(i) DIBAC–CA
Nano Luc
Halo Tag
(ii) Azido–peptides in wells prior to dispense
DμVS
Unprocessed
High BRET Signal
NB618–Az
(iii)
Lower BRET Signal
(iv)

FIG.3A

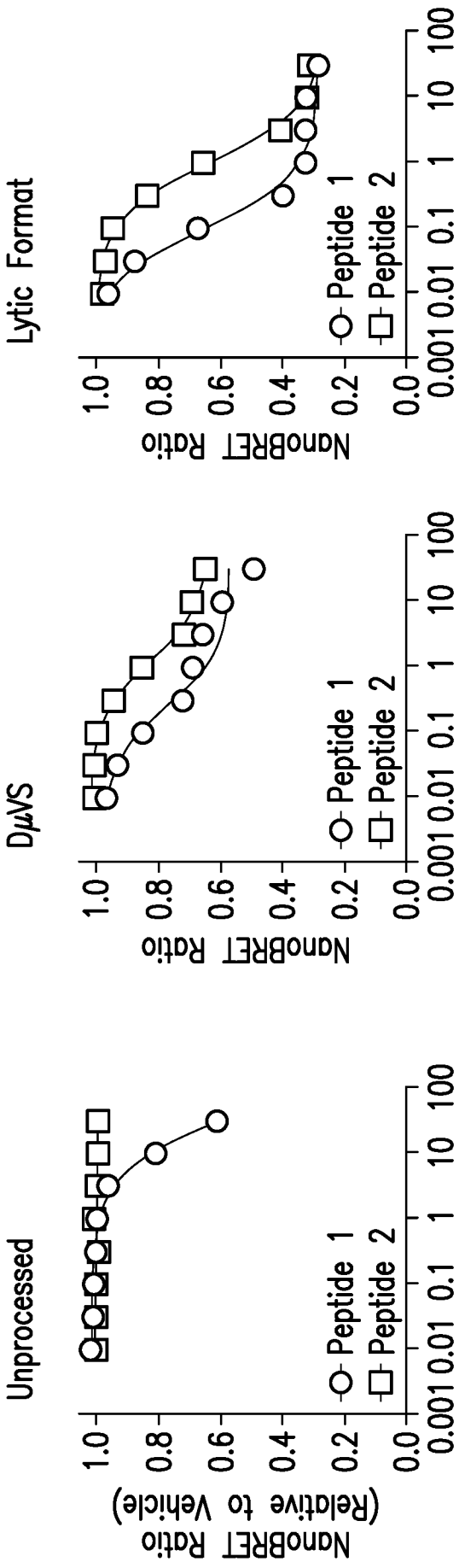

FIG.3B

FIG.3C

FIG.3D

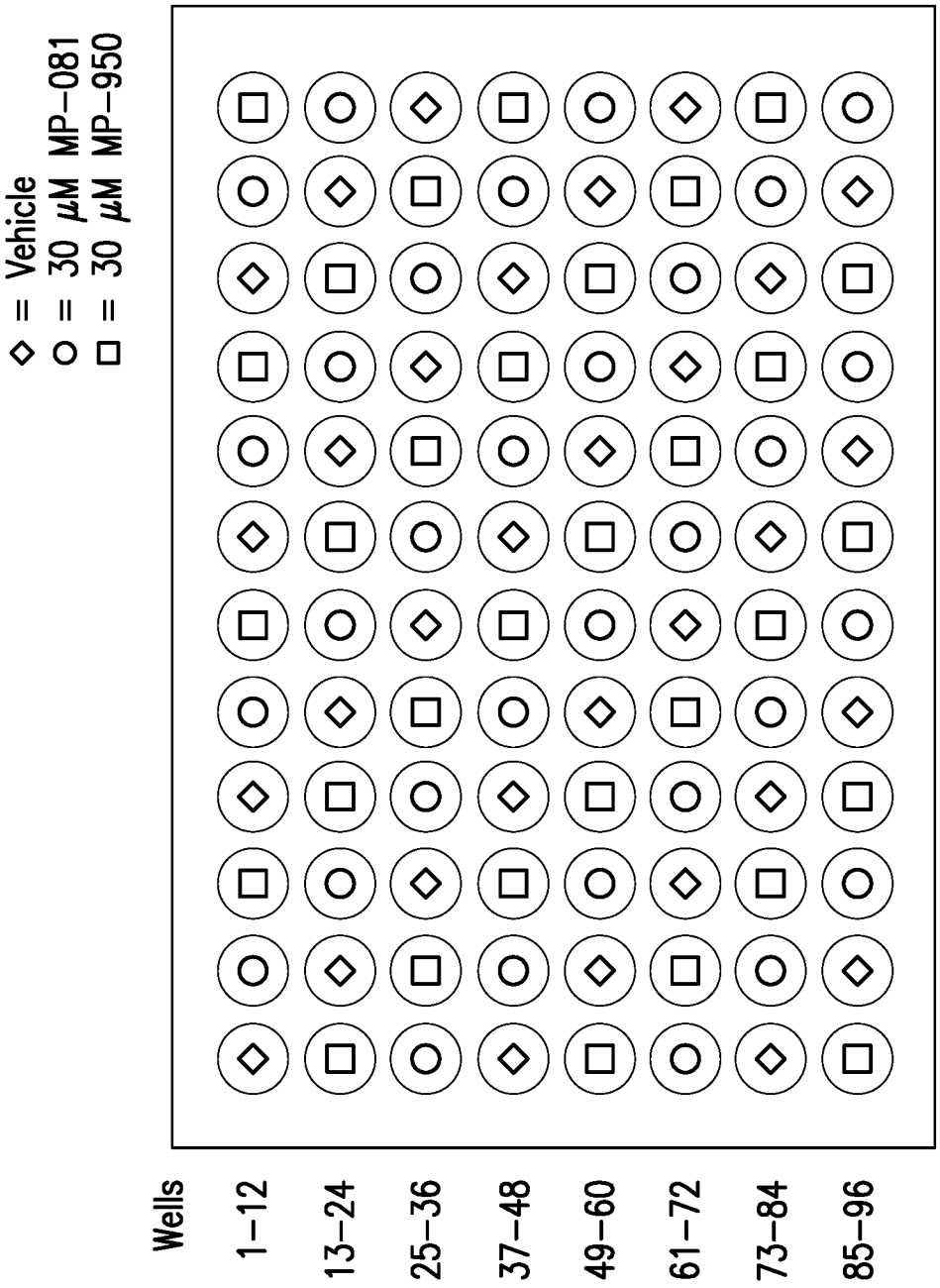
◇ = Vehicle
○ = 30 μM MP-081
□ = 30 μM MP-950
Wells
1-12
13-24
25-36
37-48
49-60
61-72
73-84
85-96

FIG.3E

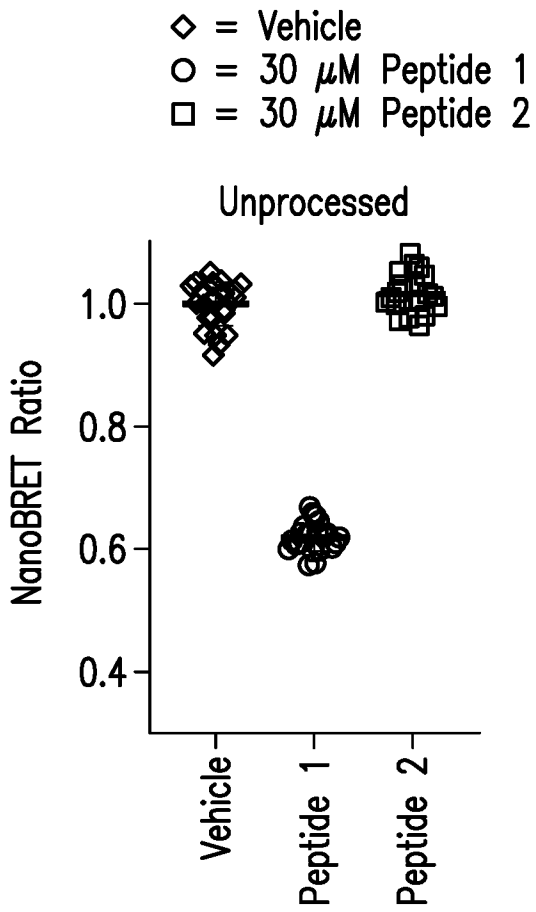
◇ = Vehicle
○ = 30 μM Peptide 1
□ = 30 μM Peptide 2
Unprocessed
NanoBRET Ratio
1.0
0.8
0.6
0.4
Vehicle
Peptide 1
Peptide 2

FIG.3F

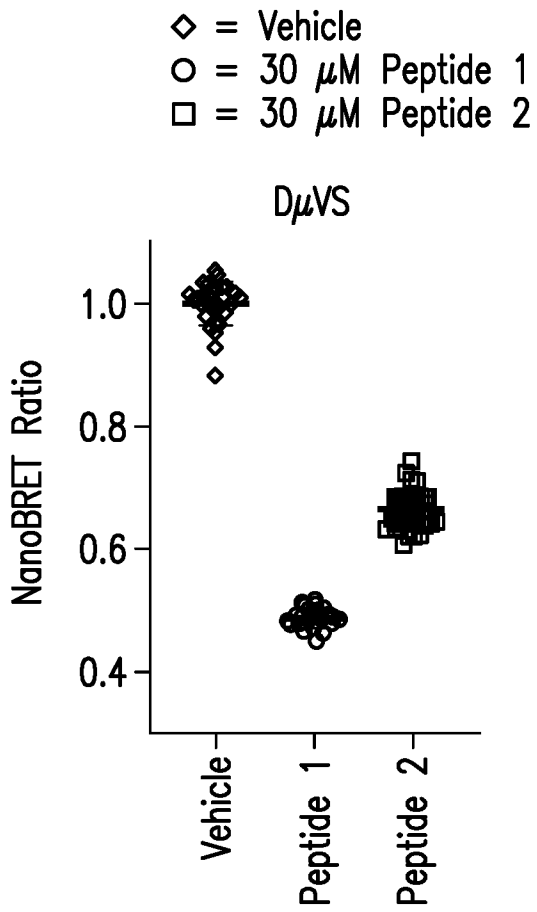
◇ = Vehicle
○ = 30 μM Peptide 1
□ = 30 μM Peptide 2
DμVS
NanoBRET Ratio
1.0
0.8
0.6
0.4
Vehicle
Peptide 1
Peptide 2

FIG.3G

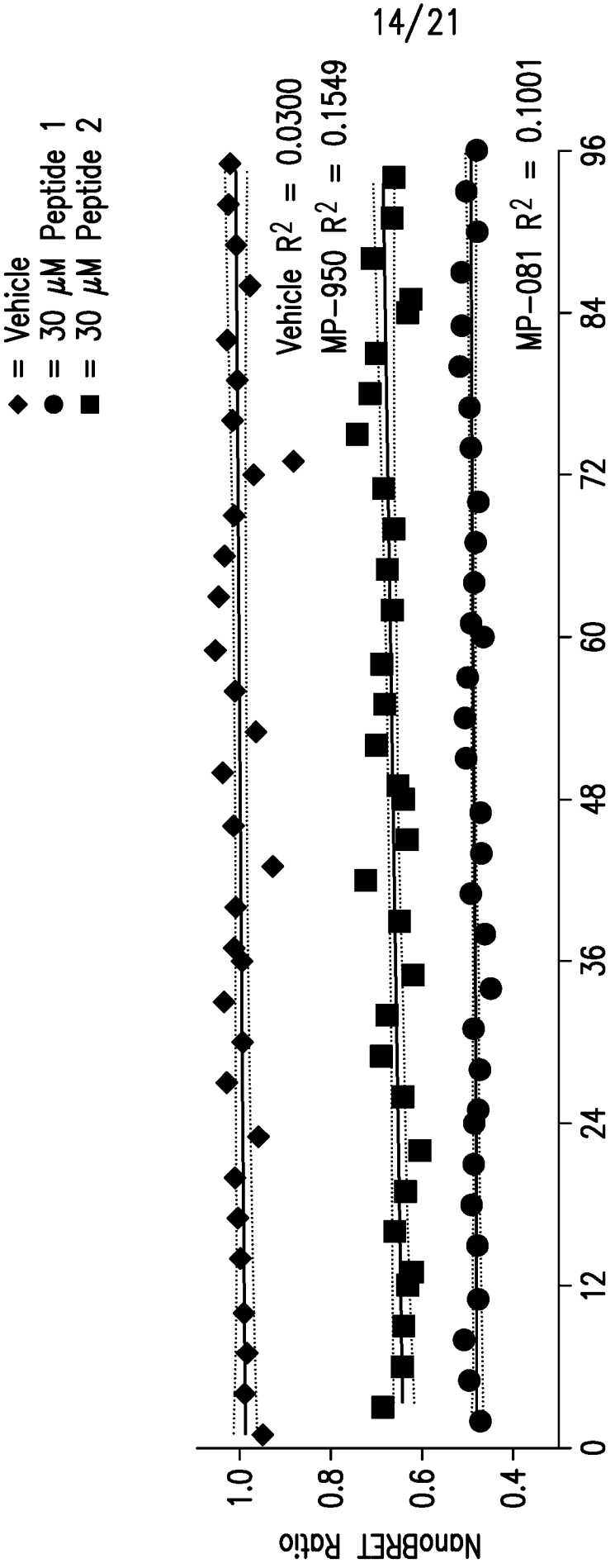
◆ = Vehicle
● = 30 μM Peptide 1
■ = 30 μM Peptide 2
Vehicle R2 = 0.0300
MP-950 R2 = 0.1549
MP-081 R2 = 0.1001
NanoBRET Ratio
1.0
0.8
0.6
0.4
0
12
24
36
48
60
72
84
96
Well Number

FIG.3H

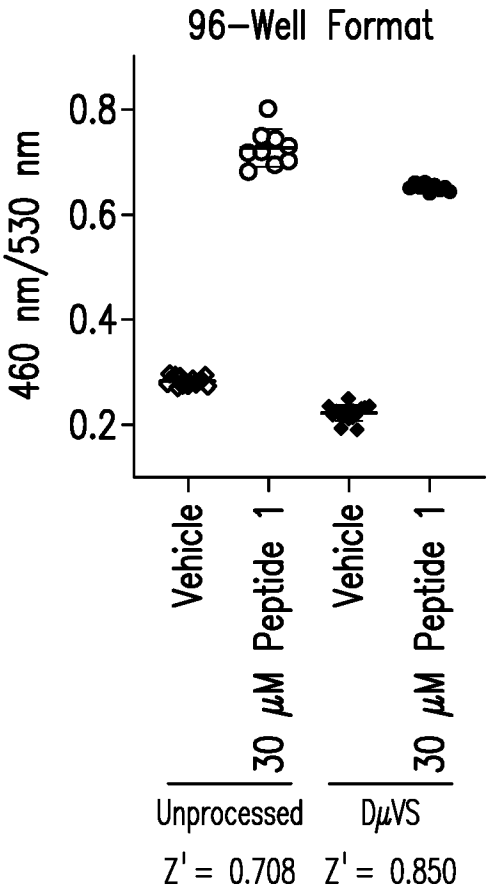
96–Well Format
460 nm/530 nm
0.8
0.6
0.4
0.2
Vehicle
30 μM Peptide 1
Vehicle
30 μM Peptide 1
Unprocessed
DμVS
Z' = 0.708
Z' = 0.850

FIG.4A

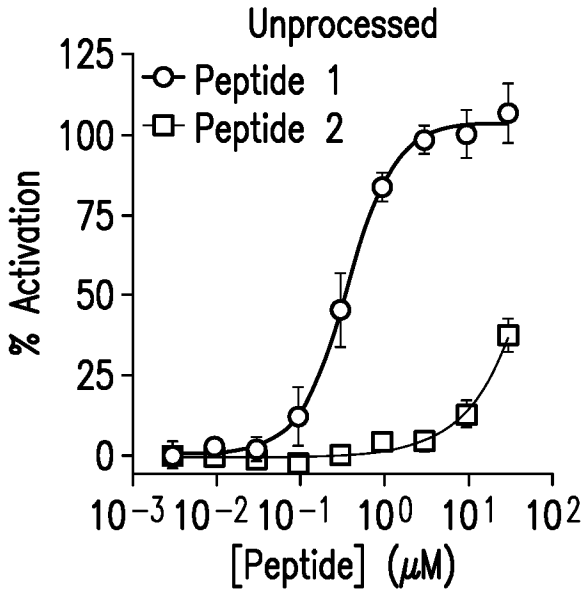
Unprocessed
Peptide 1
Peptide 2
% Activation
125
100
75
50
25
0
10−3 10−2 10−1 100 101 102
[Peptide] (μM)

FIG.4B

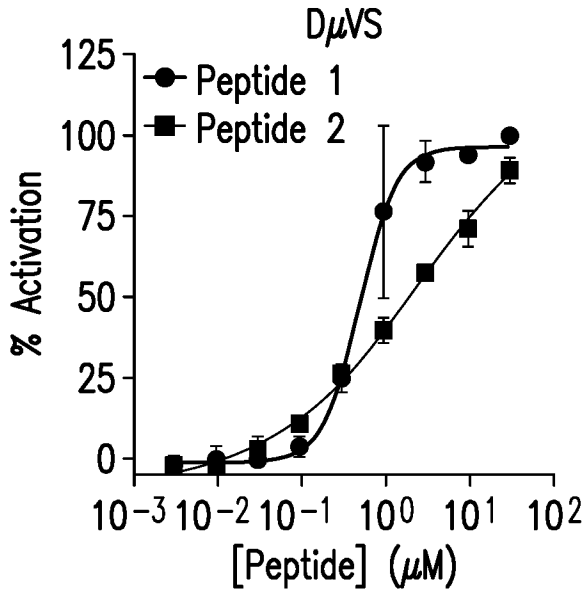
DμVS
Peptide 1
Peptide 2
% Activation
125
100
75
50
25
0
10−3 10−2 10−1 100 101 102
[Peptide] (μM)

FIG.4C

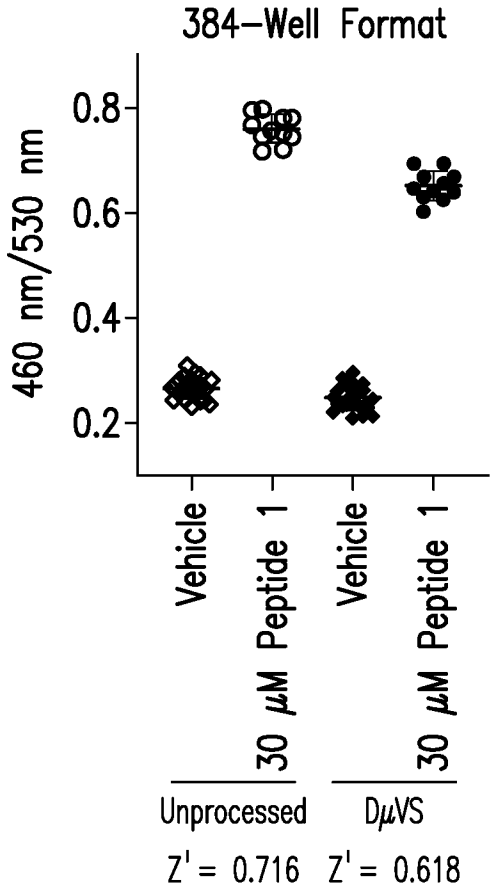
384–Well Format
460 nm/530 nm
0.8
0.6
0.4
0.2
Vehicle
30 μM Peptide 1
Vehicle
30 μM Peptide 1
Unprocessed
DμVS
Z' = 0.716
Z' = 0.618

FIG.4D

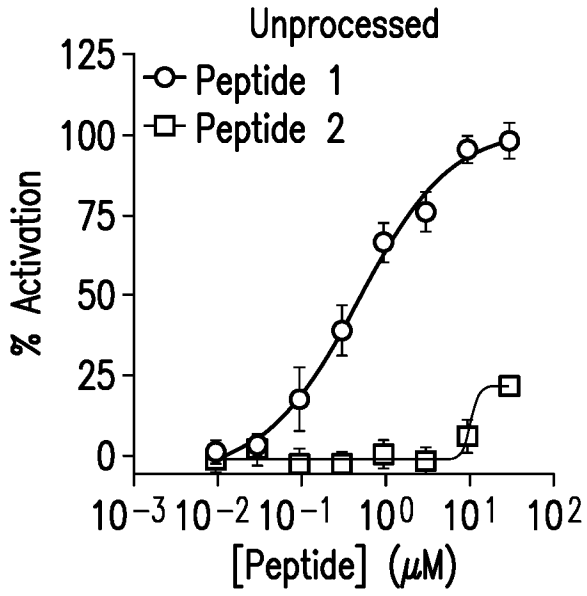
Unprocessed
Peptide 1
Peptide 2
% Activation
125
100
75
50
25
0
10^{-3} 10^{-2} 10^{-1} 10^{0} 10^{1} 10^{2}
[Peptide] (μM)

FIG.4E

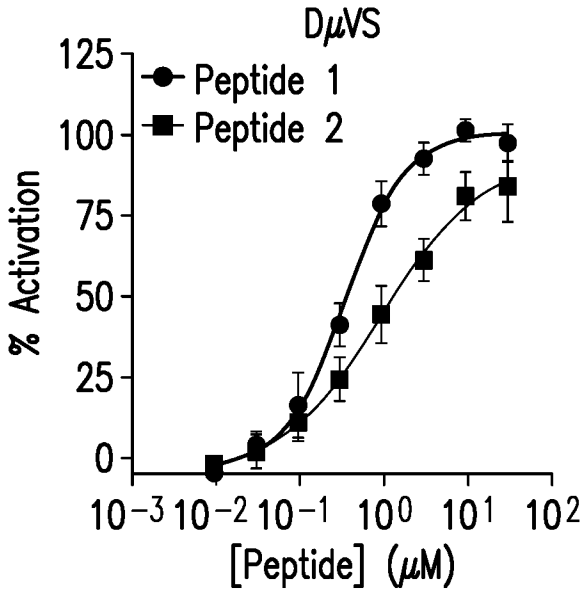
DμVS
Peptide 1
Peptide 2
% Activation
125
100
75
50
25
0
10^{-3} 10^{-2} 10^{-1} 10^{0} 10^{1} 10^{2}
[Peptide] (μM)

FIG.4F

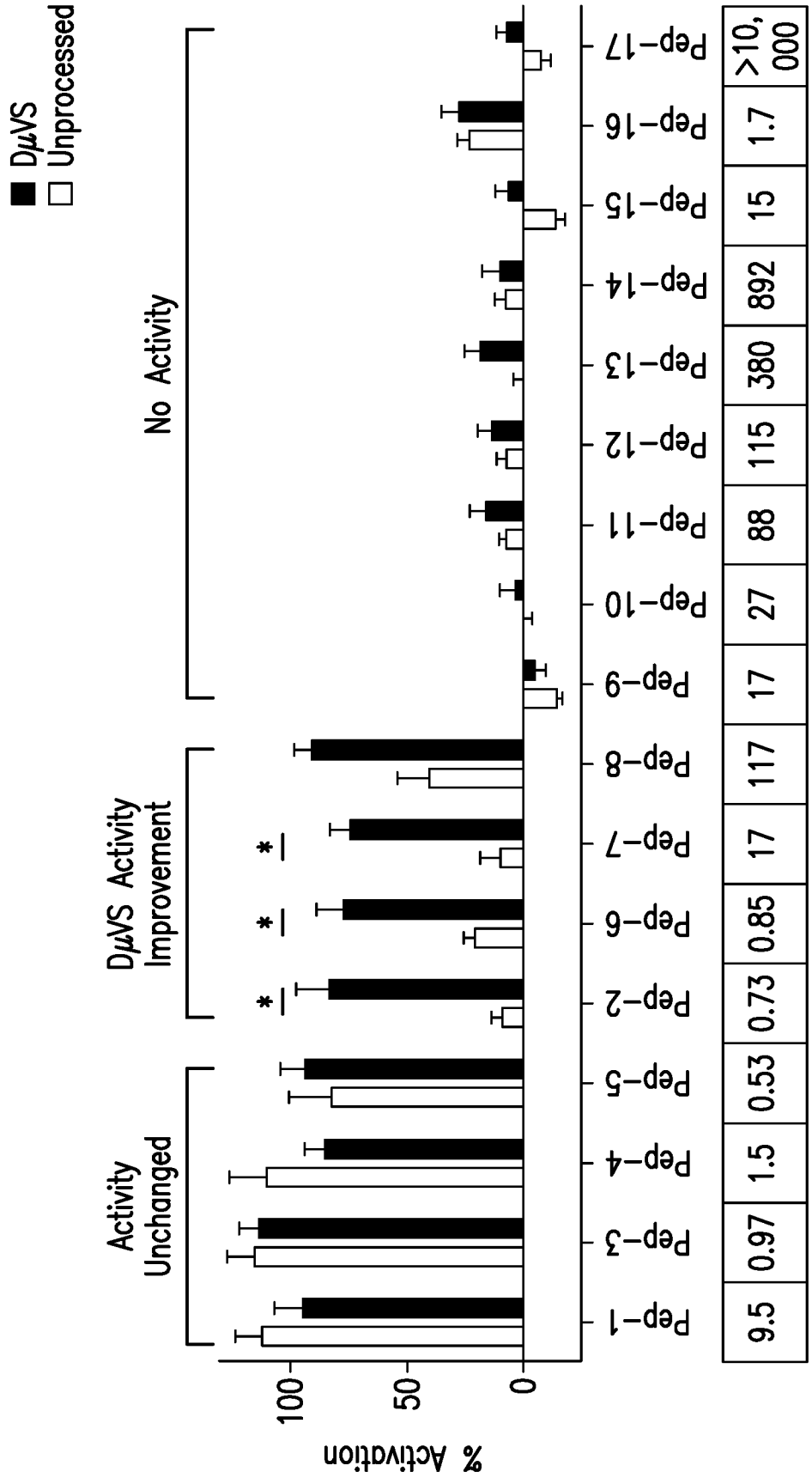
DμVS
Unprocessed
No Activity
DμVS Activity Improvement
Activity Unchanged
% Activation
100
50
0
Pep-1
Pep-3
Pep-4
Pep-5
Pep-2
Pep-6
Pep-7
Pep-8
Pep-9
Pep-10
Pep-11
Pep-12
Pep-13
Pep-14
Pep-15
Pep-16
Pep-17
*
*
*
9.5
0.97
1.5
0.53
0.73
0.85
17
117
17
27
88
115
380
892
15
1.7
>10,000

FIG.5A

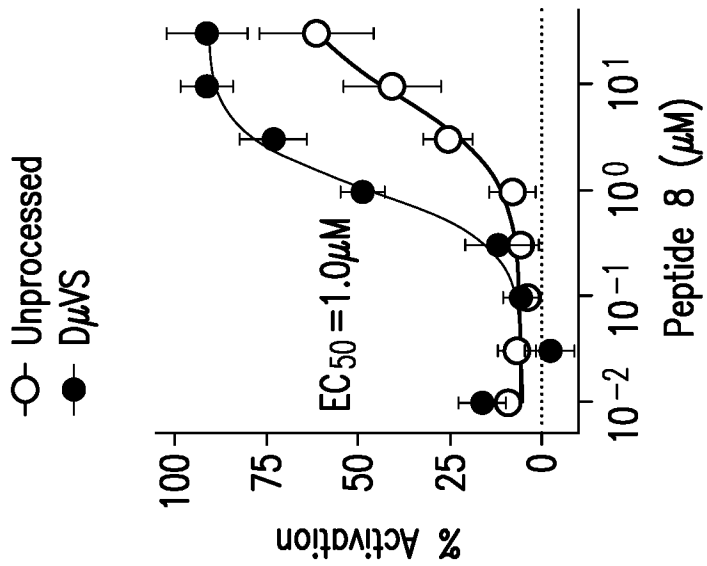

FIG.5D

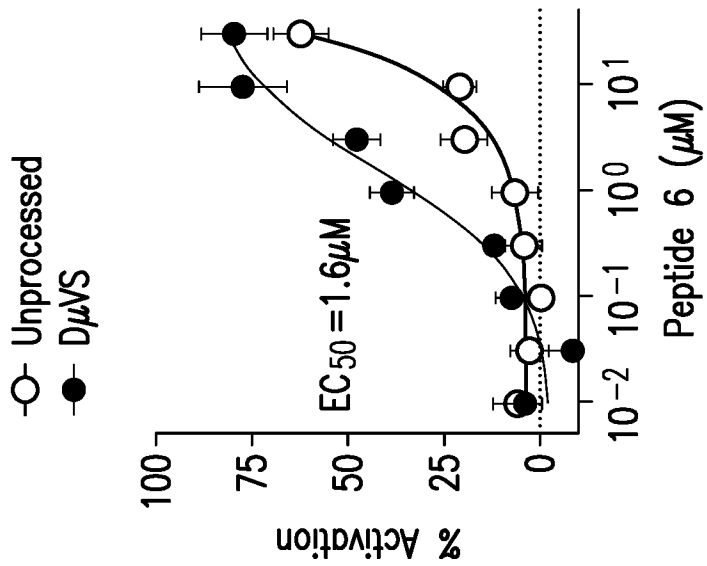

FIG.5C

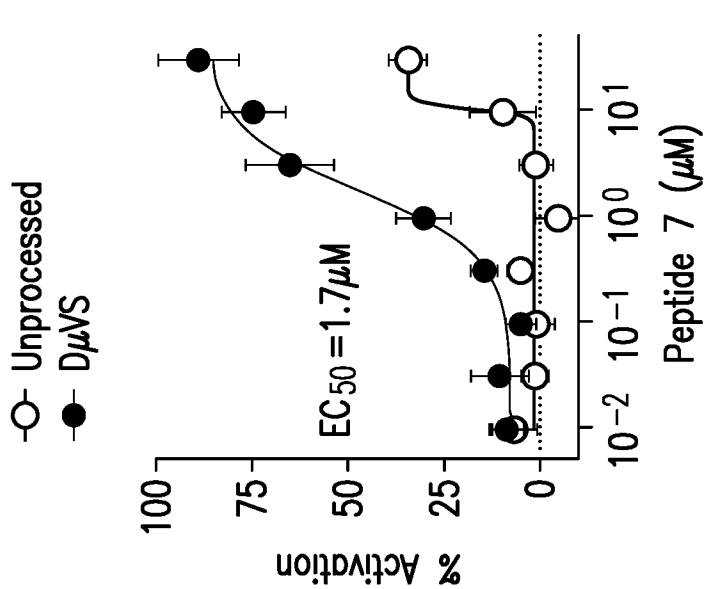

FIG.5B

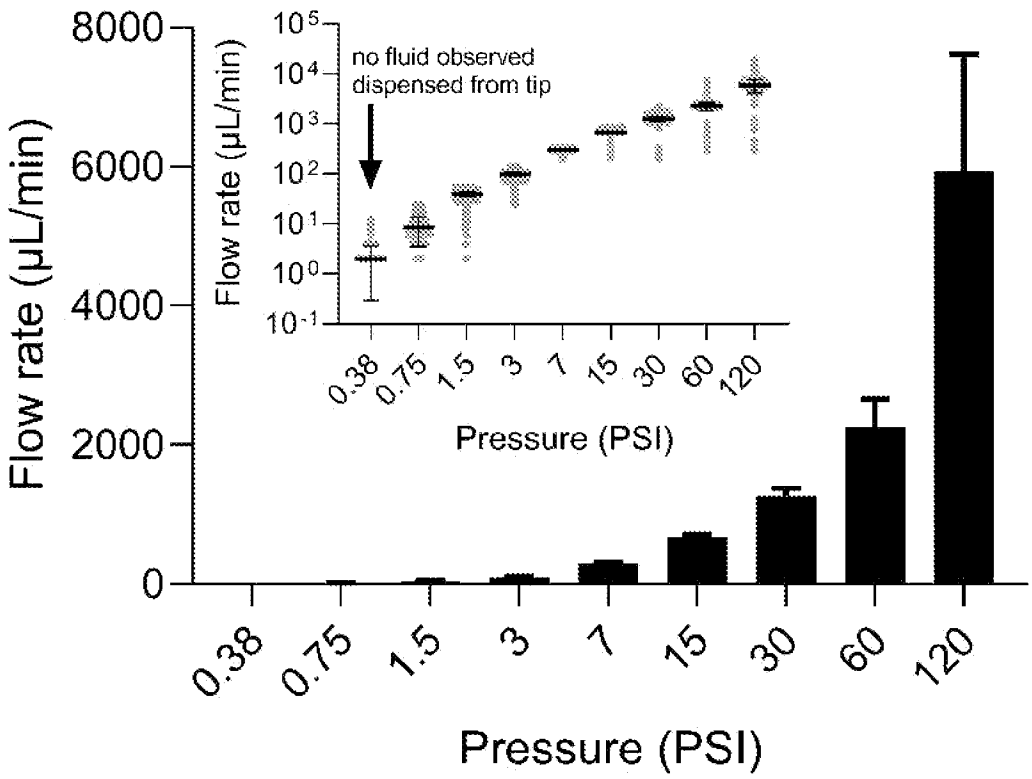
8000
6000
4000
2000
0
Flow rate (µL/min)
0.38
0.75
1.5
3
7
15
30
60
120
Pressure (PSI)
10^5
10^4
10^3
10^2
10^1
10^0
10^{-1}
Flow rate (µL/min)
no fluid observed
dispensed from tip
0.38
0.75
1.5
3
7
15
30
60
120
Pressure (PSI)

FIG. 6

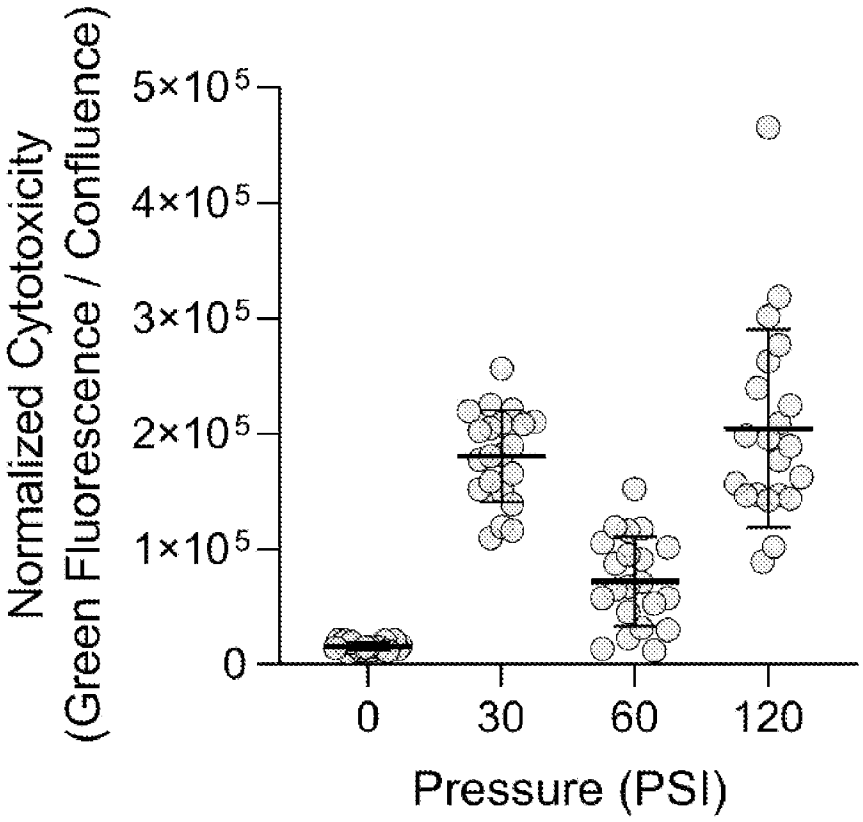
Normalized Cytotoxicity
(Green Fluorescence / Confluence)
5×10^5
4×10^5
3×10^5
2×10^5
1×10^5
0
0
30
60
120
Pressure (PSI)

FIG. 7